

ARTICLE OPEN



The Neurod1/4-Ntrk3-Src pathway regulates gonadotrope cell adhesion and motility

Charles Le Ciclé¹, Vincent Pacini^{1,4}, Nicolas Rama², Servane Tauszig-Delamasure³, Eloïse Airaud¹, Florence Petit^{1,5}, Simon de Beco⁴, Joëlle Cohen-Tannoudji¹ and David L'hôte¹✉

© The Author(s) 2023

Pituitary gonadotrope cells are essential for the endocrine regulation of reproduction in vertebrates. These cells emerge early during embryogenesis, colonize the pituitary glands and organize in tridimensional networks, which are believed to be crucial to ensure proper regulation of fertility. However, the molecular mechanisms regulating the organization of gonadotrope cell population during embryogenesis remain poorly understood. In this work, we characterized the target genes of NEUROD1 and NEUROD4 transcription factors in the immature gonadotrope α T3-1 cell model by in silico functional genomic analyses. We demonstrated that NEUROD1/4 regulate genes belonging to the focal adhesion pathway. Using CRISPR/Cas9 knock-out approaches, we established a double NEUROD1/4 knock-out α T3-1 cell model and demonstrated that NEUROD1/4 regulate cell adhesion and cell motility. We then characterized, by immuno-fluorescence, focal adhesion number and signaling in the context of NEUROD1/4 insufficiency. We demonstrated that NEUROD1/4 knock-out leads to an increase in the number of focal adhesions associated with signaling abnormalities implicating the c-Src kinase. We further showed that the neurotrophin tyrosine kinase receptor 3 NTRK3, a target of NEUROD1/4, interacts physically with c-Src. Furthermore, using motility rescue experiments and time-lapse video microscopy, we demonstrated that NTRK3 is a major regulator of gonadotrope cell motility. Finally, using a *Ntrk3* knock-out mouse model, we showed that NTRK3 regulates gonadotrope cells positioning in the developing pituitary, in vivo. Altogether our study demonstrates that the Neurod1/4-Ntrk3-cSrc pathway is a major actor of gonadotrope cell mobility, and thus provides new insights in the regulation of gonadotrope cell organization within the pituitary gland.

Cell Death Discovery (2023)9:327; <https://doi.org/10.1038/s41420-023-01615-7>

INTRODUCTION

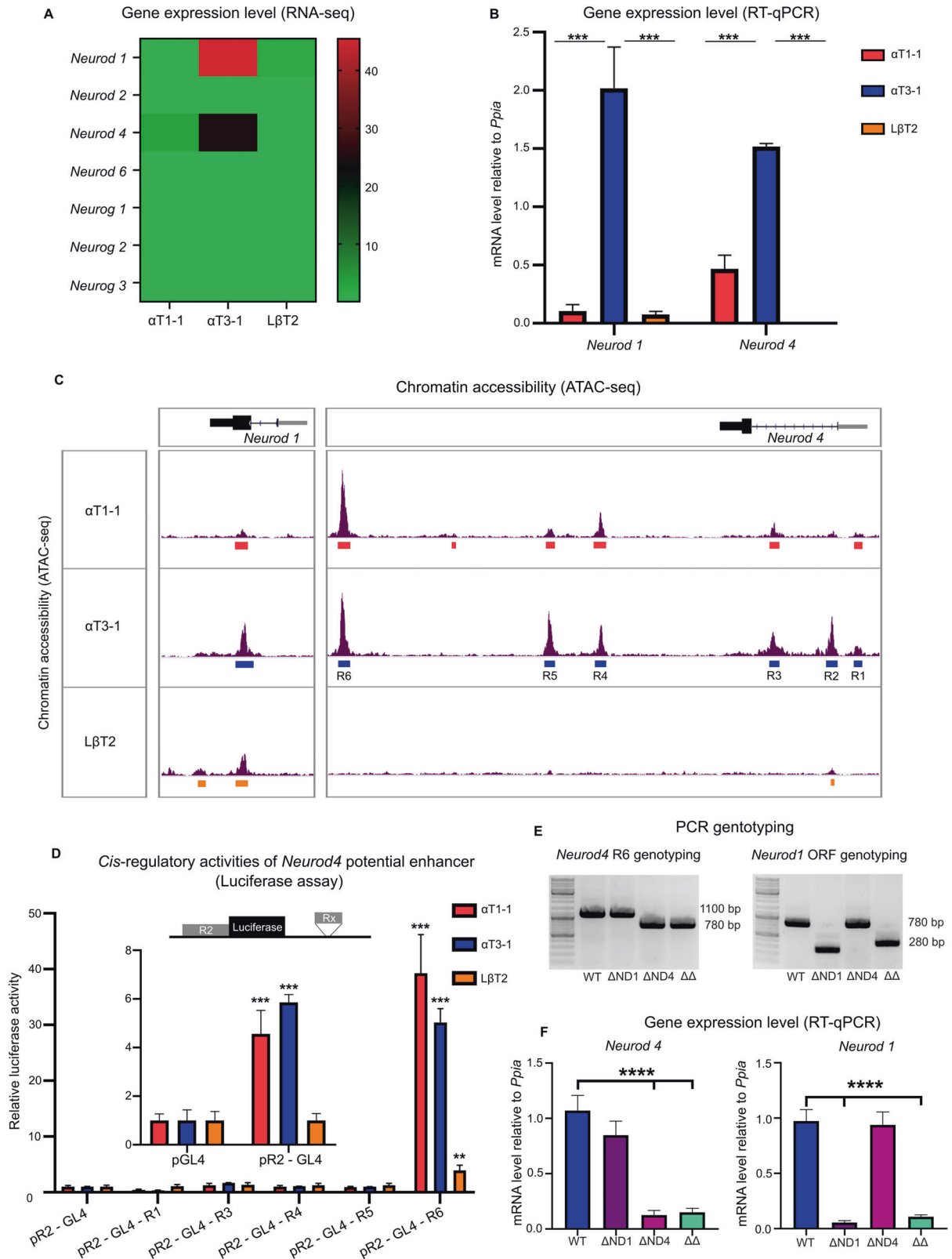
In multi-cellular organisms, the basic helix-loop-helix (bHLH) super-family regroups highly conserved transcription factors, often implicated in critical developmental processes. Amongst them, the Neurod/g sub-family emerged as major regulator of neurogenesis [1], playing critical roles in neural cell fate differentiation, but also in neuron proliferation, survival, and migration. This pro-neural sub-family is composed of four *Neurod* members: *Neurod1*, *Neurod2*, *Neurod4*, and *Neurod6* and three Neurogenin, *Neurog1*, *Neurog2*, and *Neurog3*. NEUROD1 (ND1) and NEUROD4 (ND4) along with Neurogenin factors are able to reprogram progenitor cells toward a neural fate whereas ND2 and ND6 are implicated in neuronal identity maintenance (for review [2]). These factors can functionally compensate each other, displaying partially overlapping expression patterns and sharing a highly conserved DNA binding domain [3]. Neurod/g are also involved in specification of non-neural cells such as retinal photoreceptors [4], amacrine cells [5], pancreatic endocrine β cells [6], and entero-endocrine cells [7]. Furthermore, ND1 and ND4 are known to be expressed during pituitary gland development [8–10].

The pituitary gland is a common feature of all vertebrates. The endocrine part of this gland contains six endocrine lineages in the mouse: somatotrope, lactotrope, thyrotrope, corticotrope, melanotrope and gonadotrope. Each of them secretes specific hormones implicated in the homeostatic regulation of important physiological functions. For example, the gonadotrope cells secrete the gonadotropins, LH and FSH, regulating gonadal steroidogenesis and gametogenesis and thus, fine-tuning the reproductive function. This gland differentiates from a cranial placode, at day 8.5 of embryonic development (E8.5) in the mouse [11]. Cranial placodes are tissular hotspots of cell division and morphogenesis, originating at the boundary between neural and non-neural ectoderms [12]. They are known to produce various types of migratory cells such as neural and, as more recently demonstrated, endocrine cells [13]. Interestingly, all cranial placodes are neurogenic except for anterior pituitary and lens ones, suggesting an ontogenetic proximity between neural and pituitary development. Early during embryogenesis (E9.5), the pituitary placode gives rise to the Rathke's pouch, the pituitary anlage. Progenitor cells proliferate and emigrate from this pouch to give birth to the nascent pituitary gland (around E12.5) [14].

¹Université Paris Cité, CNRS, Inserm, Unité de Biologie Fonctionnelle et Adaptative, F-75013 Paris, France. ²Centre de Recherche en Cancérologie de Lyon, Inserm U1052, CNRS UMR 5286, Centre Léon Bérard, Université Lyon1, 69008 Lyon, France. ³Institut NeuroMyoGène - CNRS UMR 5310 - Inserm U1217 de Lyon - UCBL Lyon 1, Faculté de Médecine et de Pharmacie, Lyon, France. ⁴Present address: Université Paris Cité, CNRS, Institut Jacques Monod, F-75013 Paris, France. ⁵Present address: Faculty of Pharmacy, Université de Montréal, Montréal, QC H3T 1J4, Canada. ✉email: david.lhote@u-paris.fr

Received: 20 March 2023 Revised: 8 August 2023 Accepted: 16 August 2023

Published online: 01 September 2023



From E13.5, under morphogenetic cues, the progenitors then differentiate progressively into the different endocrine lineages [15]. During this maturation, most of the pituitary lineages, and especially the gonadotrope one, are known to interconnect into cell networks [16], suggesting that cell motility might be

important to establish the complex tridimensional organization of the embryonic pituitary.

Interestingly, pituitary differentiation requires several pro-neural transcription factors, highlighting similarities between pituitary and neural development. For example, as previously mentioned,

Fig. 1 Characterization of *Neurod/g* gene expression in a model of gonadotrope cell differentiation. **A** Heatmap of *Neurod/g* gene expression in α T1-1, α T3-1, and L β T2 cells according to published RNA-seq (GSE104513). Color scale represents the normalized expression values. **B** Expression of *Neurod1* and *Neurod4* in α T1-1, α T3-1, and L β T2 cells. Gene expression levels were measured by RT-qPCR and normalized to *Ppia* (Cyclophilin A). Data are the normalized mean \pm SEM of four independent experiments. *Neurod1* and *Neurod4* transcript levels were compared between the three cell lines by ANOVA followed by Tukey multiple comparison test. $***p < 0.001$. **C** Chromatin accessibility of *Neurod1* and *Neurod4* loci in α T1-1, α T3-1, and L β T2 cells. Chromatin accessibility was investigated by ATAC-seq (assay for transposase-accessible chromatin with high-throughput sequencing) in the three gonadotrope cell lines. ATAC-seq tracks are shown for *Neurod1* (left part of the panel) and *Neurod4* (right part of the panel) loci. Gene exons are depicted as black boxes and proximal promoters are depicted as gray box in 5 prime of the ORFs. For each cell line, identified accessible chromatin regions are depicted as colored rectangles under each track. **D** *Cis*-regulatory activity of *Neurod4* potential enhancers in gonadotrope cells. α T1-1, α T3-1, and L β T2 cells were transiently transfected with a GL4 luciferase reporter cassette under the control of *Neurod4* promoter, here referred as R2 (pR2-GL4) or with this construct harboring potential *cis*-regulatory regions cloned in 3 prime of the *luciferase* cassette (pR2-GL4-Rx constructs, with x = R1 to R6 except R2). The activity of pR2-GL4 was normalized to the control pGL4 empty backbone activity (inset) and then pR2-GL4-Rx activities were normalized to pR2-GL4 activity. Relative luciferase activities are the normalized ratio between firefly luciferase over renilla luciferase. ANOVA followed by Dunnett's multiple comparison test was performed independently for each cell line. Results are the mean \pm SEM of six independent experiments. Significant difference with pR2-GL4 construct: $**p < 0.01$; $***p < 0.001$. **E** Deletion of the genomic sequence of *Neurod4* R6 enhancer and *Neurod1* ORF was carried out in α T3-1 cells using CRISPR/Cas9. For *Neurod4*, genotyping PCR amplified a 1100 bp amplicon in WT cells while stable *Neurod4* mutant cells (Δ ND4) carried a deletion of about 320 bp, removing the R6 enhancer (left part of the panel, 780 bp amplicon). For *Neurod1*, a 780 bp amplicon was detected in WT cells while stable *Neurod1* mutant cells (Δ ND1) carried a deletion of about 500 bp, which encompassed *Neurod1* ATG first codon (right part of the panel, 280 bp amplicon). The double mutant α T3-1 cell line ($\Delta\Delta$) was generated by deleting R6 enhancer on the *Neurod1* mutant background. **F** For each genotype, homozygous clones were tested for *Neurod4* and *Neurod1* expression by RT-qPCR. Gene expression levels were normalized to *Ppia*. Data are the normalized mean \pm SEM of four independent experiments. Gene expression levels of mutant clones were compared to WT by ANOVA followed by Dunnett's multiple comparison test. $****p < 0.0001$.

the pro-neural transcription factors ND1 and ND4 are expressed in the developing pituitary [8–10]. In agreement with these expression patterns, *Neurod1* or *Neurod4* knock-out leads to mild differentiation defects of corticotropes [17], lactotropes, and somatotropes, respectively [10]. While pituitary differentiation has not been investigated in *Neurod1/4* double mutant, differentiation defects of the somatotrope, corticotrope and gonadotrope lineages have been observed in a triple knock-out with *Ascl1*, coding a closely related bHLH transcription factor [18], demonstrating the importance of these factors for pituitary endocrine lineage maturation. However, the roles of ND1 and ND4, especially during gonadotrope specification, remains poorly characterized. In this work, we have studied ND1/4 molecular function during gonadotrope cell differentiation using a classical set of three immortalized mouse cell lines recapitulating three major steps of the gonadotrope differentiation process: the α T1-1 cell line, a model of early progenitors, the α T3-1 cells, exhibiting molecular signature of immature gonadotropes and finally the L β T2 cell line, representative of mature gonadotrope cells [19]. We demonstrate here that (i) ND1 and ND4 are critical factors during gonadotrope differentiation, regulating cell motility through a *Ntrk3/c-Src* pathway and (ii) NTRK3 tyrosine kinase receptor is crucial for the organization of the gonadotrope cell population during pituitary organogenesis.

RESULTS

Neurod1 and *Neurod4* are differentially expressed in a cellular model of gonadotrope differentiation

We first investigated the expression of *Neurod/g* genes in the α T1-1, α T3-1, and L β T2 cell lines. According to RNA-seq data [20], we found that *Neurod1* and *Neurod4* are the only *Neurod/g* expressed genes during gonadotrope differentiation, mostly in immature and to a lesser extent in progenitor gonadotrope cells (Fig. 1A). We confirmed this expression pattern by RT-qPCR assay (Fig. 1B). We then investigated whether *Neurod1* and *Neurod4* regulatory regions were differentially activated during gonadotrope differentiation using our published ATAC-seq data [21]. Only *Neurod1* proximal promoter displayed chromatin accessibility, mainly in immature gonadotrope cells (Fig. 1C, left part). In contrast, we found six accessible chromatin regions in *Neurod4* locus of α T1-1 and α T3-1 cells but not in L β T2 cells (Fig. 1C, right part), consistently with gene expression pattern. This indicates that *Neurod4* expression might strongly depends on several

potential enhancers scattered within the locus. We then tested enhancer *cis*-regulatory activities using luciferase reporter assays. As expected, *Neurod4* promoter region (R2) was active specifically in α T1-1 and α T3-1 cells (Fig. 1D, insert). Among the potential enhancers, only R6 dramatically increased promoter basal activity in progenitor and immature gonadotrope cells (Fig. 1D). To further demonstrate that R6 is a functional *Neurod4* enhancer, we generated stable R6 deletion in α T3-1 cells using CRISPR/Cas9 (these cells are hereafter named Δ ND4, Fig. 1E) and measured *Neurod4* expression by RT-qPCR. R6 deletion in immature gonadotropes induced a 90% decrease in *Neurod4* transcript levels (Fig. 1F), demonstrating that the R6 enhancer is necessary for *Neurod4* expression in α T3-1 cells. To our knowledge, this *Neurod4* enhancer had not been described yet. As this evolutionary conserved region displays chromatin accessibility in tissues such as brain and retina (according to the UCSC Genome Browser databases), it might also be a critical *Neurod4* regulatory region beyond the pituitary gland. The Δ ND4 cells can be considered as an immature gonadotrope *Neurod4* knock-out cellular model, allowing the analysis of ND4 functions in this cell type.

To study ND1 roles in immature gonadotropes, we created a α T3-1 *Neurod1* mutant cell line by deleting the first ~500 bp of the *Neurod1* ORF with CRISPR/Cas9 (Fig. 1E, Δ ND1 cells), which successfully abolished gene expression (Fig. 1F). Finally, in order to investigate potential functional compensations between the two NEUROD factors, we established a double mutant α T3-1 cell line by deleting *Neurod4*-R6 in Δ ND1 cells (Fig. 1E, $\Delta\Delta$ cells) leading to a strong down-expression of both *Neurod1* and *Neurod4* (Fig. 1F).

Characterization of NEUROD1 and NEUROD4 potential regulome in immature gonadotrope cells

In order to characterize the molecular function of ND1 and ND4 in α T3-1 cells, we conducted an in silico functional genomics analysis (Fig. 2A). By cross-referencing several databases, we identified α T3-1 cells expressed genes (RNA-seq data [20]) associated with potential *cis*-regulatory regions displaying chromatin accessibility (α T3-1 cells ATAC-seq [21]) also known to be ND1 targets in other cell types (ND1 ChIP-seq data retrieved from <https://chip-atlas.org/> [22]).

In order to validate ND1/4 potential target genes identified in α T3-1 cells by this in silico approach, we measured the expression of a sample of them by RT-qPCR in WT, Δ ND1, Δ ND4, and $\Delta\Delta$ cells (Fig. 2B). The expression of 40% of these genes was significantly

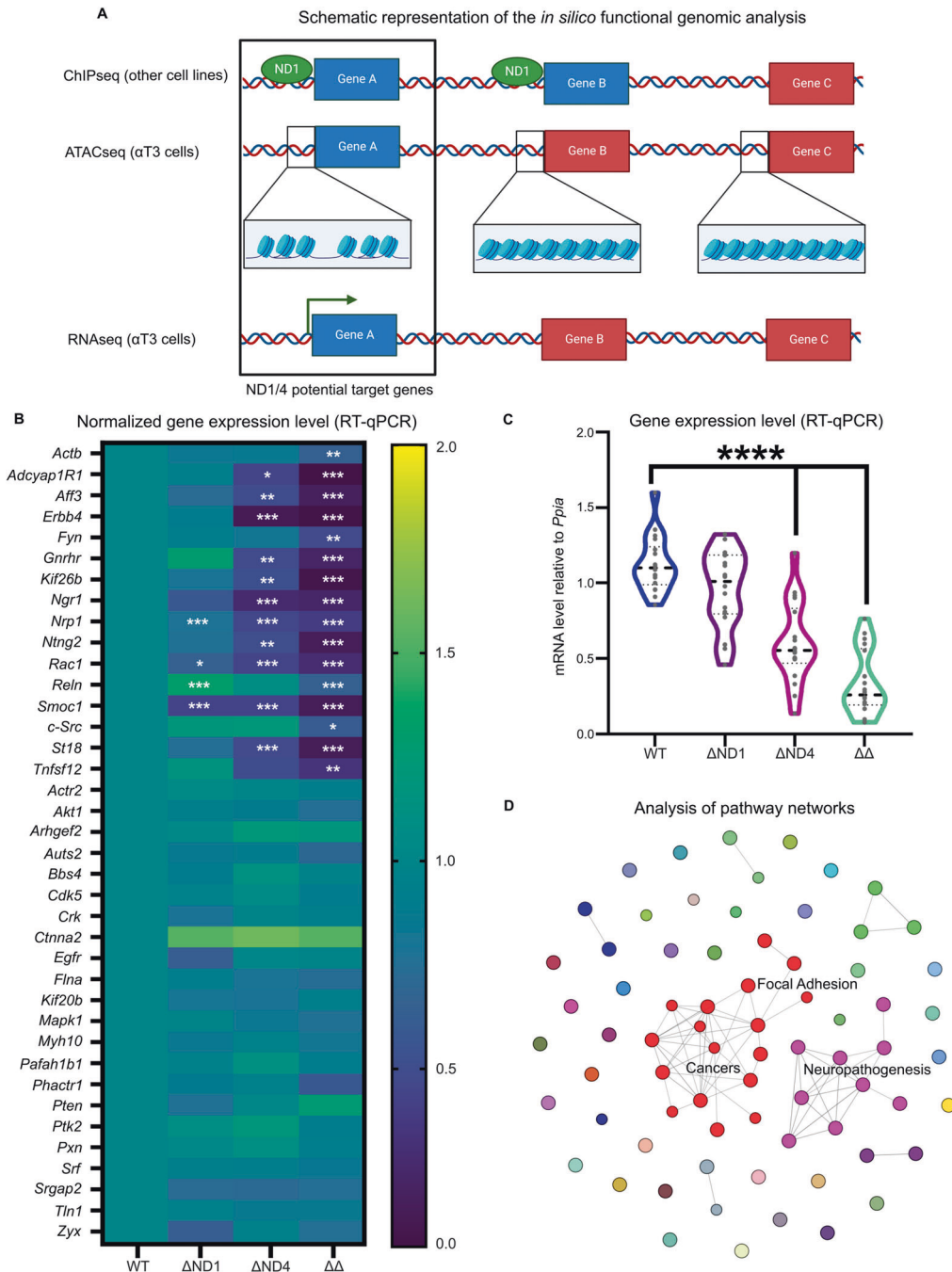
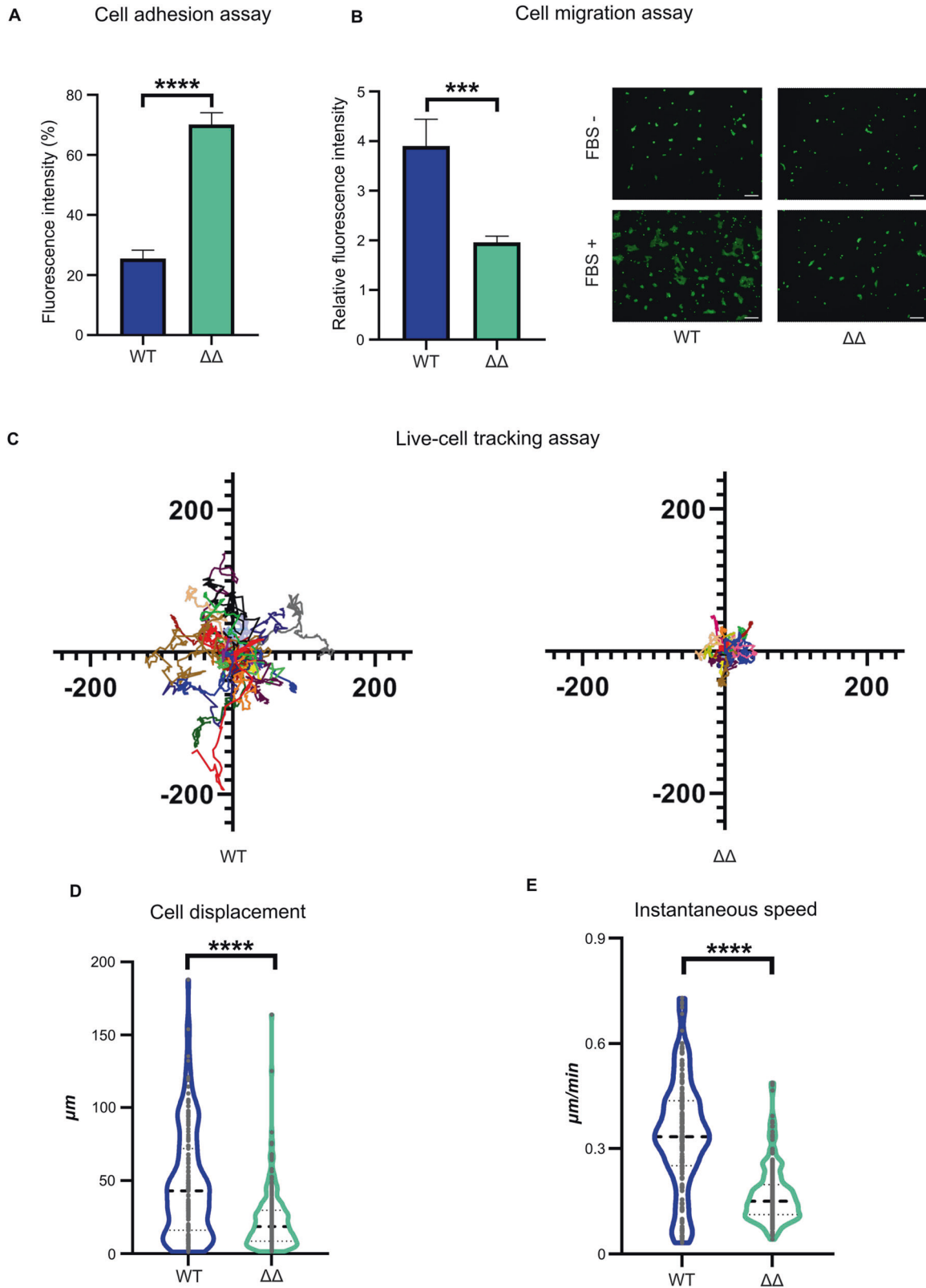


Fig. 2 Characterization of the ND1/4 potential regulome in α T3-1 cells. **A** Schematic representation (created with BioRender) of the *in silico* functional genomics analysis used to identify ND1/4 potential target genes in α T3-1 cells. Expressed genes associated with genomic regions displaying chromatin accessibility and potentially directly targeted by NEUROD factors were identified by cross-referencing ND1 ChIP-seq (from heterologous cell types) with α T3-1 cell ATAC-seq and RNA-seq databases. Retained candidate genes are depicted using blue boxes whereas discarded genes are depicted by red boxes. **B** Heatmap of the expression of 38 ND1/4 potential target genes identified *in silico*, in WT, Δ ND1, Δ ND4, and $\Delta\Delta$ cells. Gene expression levels were normalized to *Ppia*. Color scale represents the normalized expression mean of four independent experiments. Gene expression in Δ ND1, Δ ND4, $\Delta\Delta$ cells were compared to WT (values set to 1) by ANOVA followed by Dunnett's multiple comparison test. * $p < 0.05$, ** $p < 0.01$, and *** $p < 0.001$. **C** Violin plots of relative mRNA levels of 16 identified ND1/4 bona fide target genes (genes with significant expression decrease) according to WT, Δ ND1, Δ ND4, or $\Delta\Delta$ genotype. To assess the global effect of *Neurod1* and *Neurod4* deletion on gene expression, mean expression levels of the target genes in Δ ND1, Δ ND4, and $\Delta\Delta$ genotypes were compared to WT using an ANOVA followed by Dunnett's multiple comparison test. **** $p < 0.0001$. **D** Network pathway analysis representation using Cytoscape ClueGO software. Analysis was performed on potential ND1/4 target genes identified by the genomic *in silico* analysis. Each colored dot is a different pathway regrouping several potential ND1/4 target genes. Related pathways (sharing more than 25% of their genes) are connected by a gray line. Pathways in the same cluster share a common color. Pathway's name and associated genes are described in supplementary table 1.



decreased in $\Delta\Delta$ cells as compared to WT, indicating that the *in silico* approach successfully captured a significant proportion of ND1/4 targets in α T3-1 cells. To compare the mean effect of ND1 and ND4 deletion on regulation of gene expression, we plotted the extent of variation according to the cell genotypes (Fig. 2C). This revealed that ND4 might play a more critical role as a

transcriptional regulator as compared to ND1 in gonadotrope cells, even if ND1 may still be able to compensate in part for ND4 insufficiency ($\Delta\Delta$ vs Δ ND4 cells, $p < 0.01$).

To identify ND1/4 functions in gonadotrope cells, we then performed a network pathway enrichment analysis on their potential target genes, using Cytoscape ClueGO software [23]. We

Fig. 3 Regulation of α T3-1 cell adhesion and motility by ND1/4. **A** Cell adhesion assay. Fluorescent Calcein AM-labeled WT and $\Delta\Delta$ cells were seeded on an uncoated 96-well transparent bottom plate for 30 min. Fluorescence intensity is the ratio of fluorescence after PBS flushing over the initial fluorescence, reflecting the fraction of attached cells. Data are the normalized mean \pm SEM of 3 independent experiments. The % of $\Delta\Delta$ attached cells was compared to the one of WT using a Student's *t* test. *****p* < 0.0001. **B** FluoroBlok transwell migration assay. Calcein AM-labeled WT and $\Delta\Delta$ cells were seeded in FluoroBlok transwell inserts and treated with foetal bovine serum (FBS, 10% in DMEM). Left: Relative Fluorescence Unit is the ratio of post-migratory fluorescence of FBS treated over untreated cells. Data are the normalized mean \pm SEM of 6 independent experiments. Migration of $\Delta\Delta$ cells was compared to WT using a Student's *t* test. ****p* < 0.001. Right: Representative images of post-migratory fluorescent WT and $\Delta\Delta$ cells with or without FBS as chemoattractant. scale bar = 100 μ m. **C** Live-cell tracking assay. WT and $\Delta\Delta$ cells were transfected with H2B-mCherry to label and track the nuclei. Cells were seeded on Matrigel-coated culture surface until attachment and cell motility was tracked using live video time-lapse microscopy over 16 h. Tracks were analyzed using ImageJ TrackMate. Each graph corresponds to 30 representative tracks of transfected WT or $\Delta\Delta$ cells with the initial position of the cells centered at the origin. Units: μ m. **D** Total cell displacement analysis. The total distance (in μ m) traveled by cells over 16 h was analyzed using ImageJ TrackMate on 150 WT and 220 $\Delta\Delta$ cells. $\Delta\Delta$ cell mean displacement was compared to WT. *****p* < 0.0001 (Mann–Whitney test). **E** Cell velocity analysis. Cell instantaneous speed (nm/s) was calculated from the analysis of 150 WT and 220 $\Delta\Delta$ cells using ImageJ TrackMate. $\Delta\Delta$ cell mean velocity was compared to WT. *****p* < 0.0001 (Mann–Whitney test).

identified 72 significantly enriched pathways (Fig. 2D and supplementary table 1) organized in two major networks: one clustering neuro-pathogenesis-related pathways, consistently with known ND1/4 functions, and a second network of cancer and focal adhesion-related pathways.

NEUROD1/4 regulate gonadotrope cell adhesion and motility

The *in silico* analysis suggests that ND1/4 could be implicated in the regulation of focal adhesion (FA) organization and thus in adhesion and motility of gonadotrope cells. In order to test such hypothesis, we first performed a cell attachment assay using WT and $\Delta\Delta$ cells. We found a 3-fold increase in $\Delta\Delta$ cell attachment as compared to WT cells (Fig. 3A), suggesting that ND1/4 contribute to the regulation of cell interaction with the culture surface. Given that cell-matrix adhesion is involved in cell motility, we then performed a transwell migration assay using fetal bovine serum (FBS) as chemo-attractant. We observed that $\Delta\Delta$ cells displayed a significant 2-fold migration decrease (Fig. 3B) whereas migration was unaltered in Δ ND1 and Δ ND4 cells (supplementary Fig. S1).

In order to further characterize cell motility, we analyzed WT and $\Delta\Delta$ cell velocity and overall cell displacement using video time-lapse microscopy. While α T3-1 WT cells were motile, $\Delta\Delta$ cells only wobbled at their initial position (Fig. 3C and supplementary movies M1 and M2). We observed a significant ~50% decrease of both parameters in $\Delta\Delta$ cells (Fig. 3D, E), indicative of cell motility impairment.

Altogether, these results demonstrate, for the first time, that ND1/4 are critical regulators of motility and adhesion of immature gonadotropes cells.

NEUROD1/4 regulate focal adhesion number

To test the potential regulation of FAs by NEUROD1/4, we first immuno-stained key components of FAs such as vinculin (VIN), FA kinase (FAK) or Zyxin (ZYX) in WT and $\Delta\Delta$ cells. F-actin cytoskeleton was labeled using Phalloidin-TRITC. F-actin, FAK, and VIN can be considered as constitutive elements of all types of FAs, whereas ZYX is described as a marker of mature FAs [24]. We observed a 50% decrease of F-actin cellular content in $\Delta\Delta$ cells (Fig. 4A, E), consistent with the decrease in *Actb* expression (Fig. 2A). Yet, actin-based cytoskeleton structures were still observable overall. This analysis also revealed a significant 40% reduction of mean apparent cell area in $\Delta\Delta$ cells (Fig. 4F), suggesting a reduction of cell spreading. To analyze FAs more specifically, we first immuno-localized VIN and observed a significant 35% increase in number of Vinculin patches in $\Delta\Delta$ cells without variation of global signal intensity (Fig. 4B, G, H). This suggests that FA number is increased in $\Delta\Delta$ cells, in line with cells being more adherent and also less motile. To rule out the involvement of other structures implicated in cell adhesion and motility such as lamellipodia and invadopodia, we also analyzed Cortactin distribution which showed no difference between WT and $\Delta\Delta$ cells (supplementary Fig. S2). We then analyzed the

distribution pattern of total FAK and observed a comparable nucleo-cytoplasmic staining with signal at FAs in WT and $\Delta\Delta$ cells (Fig. 4C, I). This suggests that FAK is similarly expressed in both cell lines. This was further confirmed by RT-PCR and western blotting (supplementary Fig. S3A, B). Finally, we analyzed the distribution pattern of the mature FA marker ZYX (Fig. 4D, J, K). We found an unchanged number of ZYX-labeled FA in $\Delta\Delta$ cells despite a significant 35% decrease in ZYX global cell content, suggesting that $\Delta\Delta$ cells might accumulate immature FAs.

Altogether, these results thus indicate that ND1/4 regulate actin cytoskeleton organization and FA number in gonadotrope cells and might be implicated in FA maturation.

NEUROD1/4 regulate focal adhesion signaling

FA maturation is known to be regulated by phosphorylation of several effectors, such as FAK and c-Src. Briefly, upon stimulation, FAK dimerizes and auto-phosphorylates on Y³⁹⁷ residue (as reviewed in [25]). Activated c-Src is then recruited at FAs and, acting as a scaffold, independently of any catalytic activity, facilitates Y⁸⁶¹ phosphorylation and full FAK activation by Y^{576/577} phosphorylation [26]. c-Src catalytic activity is then required for FAK Y⁹²⁵ phosphorylation [26], promoting FA turn-over [27].

We analyzed here both FAK phosphorylation level and cellular distribution for all aforementioned phosphorylation marks. We observed a significant increase in the number of FAs positive for pY³⁹⁷, pY^{576/577}, and pY⁹²⁵ FAK in $\Delta\Delta$ cells (Fig. 5A–D, F, H, J), consistently with the overall increase in FA number in these cells. Concerning FAK phospho-forms cellular content, we observed a complex perturbation pattern in $\Delta\Delta$ cells: pY⁸⁶¹ level was similar between $\Delta\Delta$ and WT cells, while both pY³⁹⁷ and pY⁹²⁵ were significantly decreased and pY^{576/577} was significantly increased in $\Delta\Delta$ cells (Fig. 5E, G, I, K). Similar level in FAK pY⁸⁶¹ rules out a systematic impairment of FAK phosphorylation. Decreased level of pY³⁹⁷ might suggest a defect of FAK early activation and might be due to a lesser cell spreading (Fig. 4F) and subsequent integrin activation. However, increased level of pY^{576/577} might indicate a secondary hyper-activation of FAK and suggests that c-Src scaffolding activity is intact in these cells. Finally, decrease in pY⁹²⁵ level is consistent with a defect in FA late maturation and suggests an impairment in c-Src kinase activity. Altogether these results suggest that FA maturation defect might disturb FAK phosphorylation dynamics. To better understand this complex perturbation pattern, we then investigated c-Src activation.

At the basal state, c-Src is phosphorylated on Y⁵²⁷, a repressive post translational modification. Dephosphorylation of pY⁵²⁷ is necessary for c-Src auto-phosphorylation on Y⁴¹⁶ which leads to its activation [28]. We thus analyzed total and phosphorylated c-Src localization in WT and $\Delta\Delta$ cells (Fig. 5L–R). Total and pY⁵²⁷c-Src displayed a cytoplasmic localization whereas pY⁴¹⁶c-Src localized at FAs. We observed a significant, albeit slight, decrease in total or pY⁵²⁷c-Src contents between WT and $\Delta\Delta$ cells, whereas there was an unexpected 50% decrease of

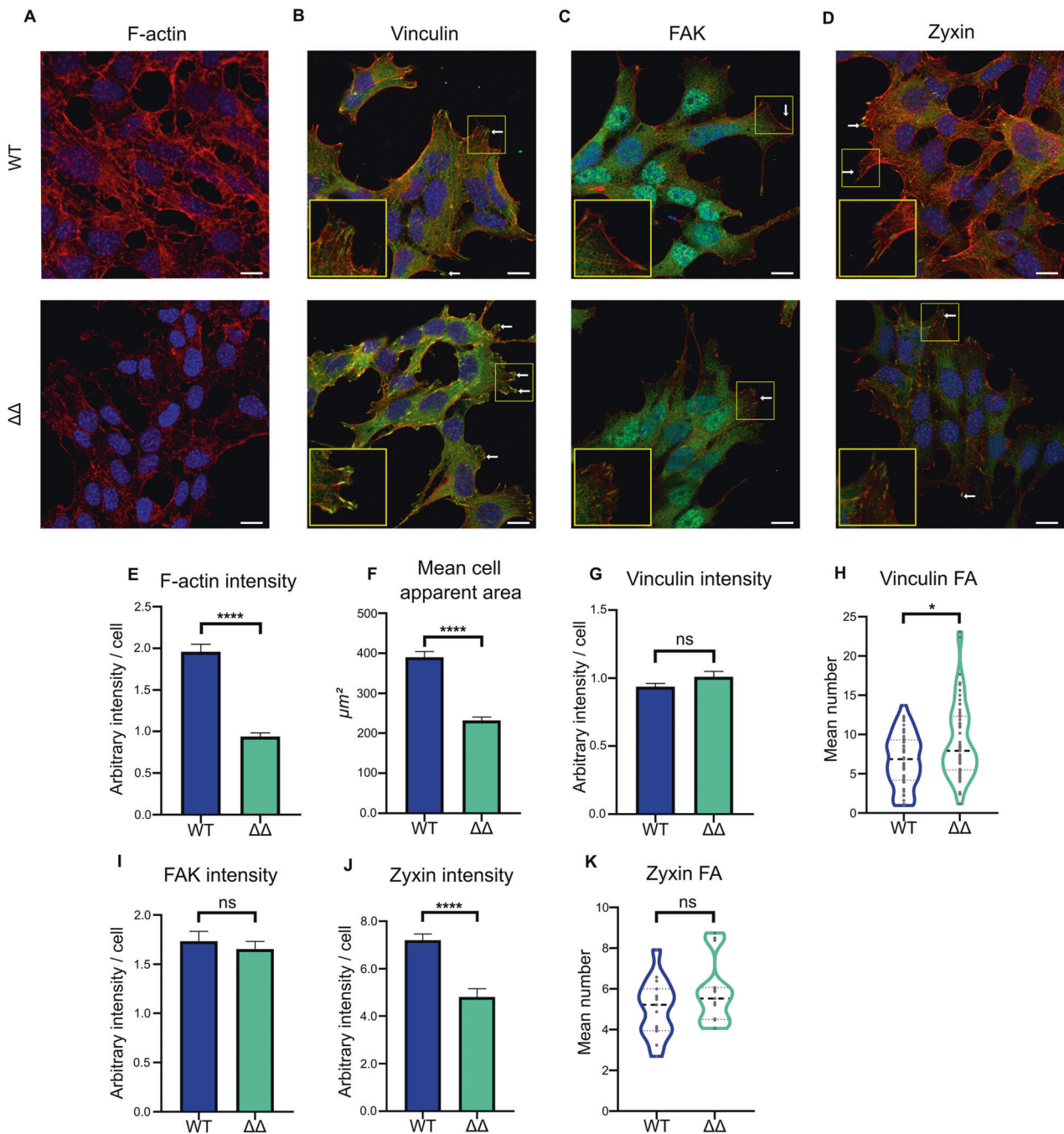
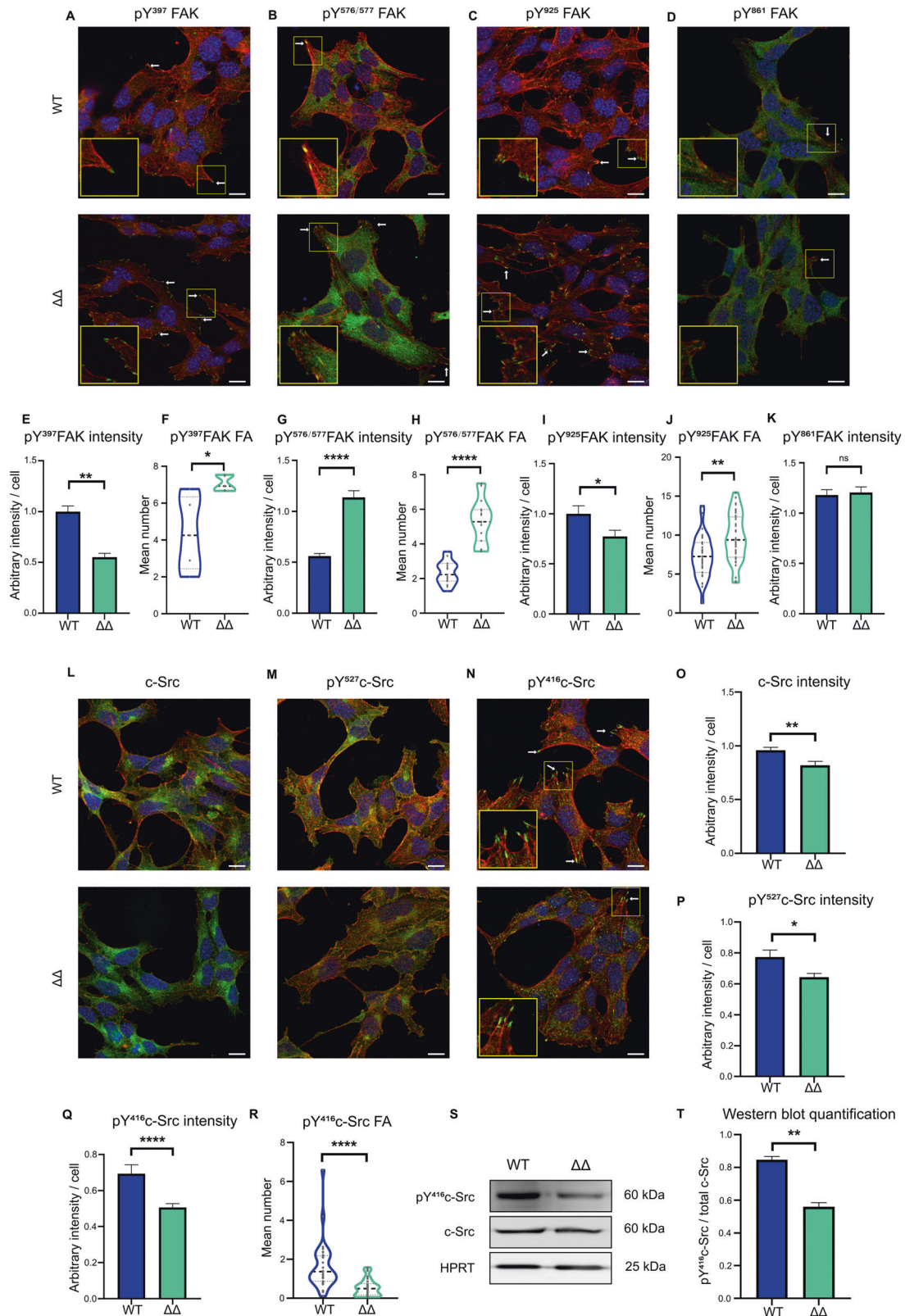


Fig. 4 Subcellular localization of actin, vinculin, FAK, and zyxin in WT and $\Delta\Delta$ cells. **A–D** Representative confocal images of **A** F-actin, **B** VIN, **C** FAK, and **D** ZYX-labeled WT and $\Delta\Delta$ cells. Fixed cells were labeled using phalloidin-TRITC for F-actin and DAPI for nuclei (Red: F-actin, Blue: nuclei, Green: VIN, FAK, or ZYX). **B, D** White arrows indicate positive **B** VIN and **D** ZYX-labeled FAs. Areas boxed in yellow are presented in the insets. scale bar = 10 μm . **E** Bar graphs of the mean F-actin fluorescence per cell and **F** mean cell apparent area, quantified on 30 different images for each genotype. **** $p < 0.0001$ (Mann–Whitney test). **G** Bar graphs of the mean VIN fluorescence intensity per cell and **H** violin plots of VIN-labeled FA particle number, quantified on 50 different images for each genotype. Mean VIN intensity and number of VIN-positive FAs were compared between $\Delta\Delta$ and WT cells. * $p < 0.05$ and ns: not significant (Mann–Whitney test). **I** Bar graph of the mean FAK signal fluorescence intensity per cell, quantified on 15 different images for each genotype. Mean cell FAK intensity was compared between $\Delta\Delta$ and WT cells. ns: not significant (Mann–Whitney test). **J** Bar graph of the mean ZYX signal fluorescence intensity per cell and **K** violin plots of ZYX-labeled FA particle numbers were quantified on 15 different images for each genotype. ZYX- mean cell intensity and number of ZYX-positive FAs were compared between $\Delta\Delta$ and WT. **** $p < 0.0001$ and ns: not significant (Mann–Whitney test).

pY⁴¹⁶ labeled-FAs in $\Delta\Delta$ cells. Hypo-phosphorylation of c-Src on Y⁴¹⁶ was confirmed by western blot (Fig. 5S, T). The c-Src activation defect is consistent with the FAK phosphorylation pattern described above, suggesting that ND1/4 are implicated in c-Src activation and hence in FA organization.

NEUROD1/4 regulate gonadotrope cell motility through c-Src activation

To link c-Src hypo-activation to motility defect of $\Delta\Delta$ cells, we first over-expressed WT, dominant negative (DN) K297R/Y527F or constitutively activated (CA) Y527F c-Src in $\Delta\Delta$ cells and monitored



cell motility using video time-lapse microscopy (Figs. 6A and S4A, B). While DN c-Src had no effect, we observed that over-expression of WT c-Src fully rescued cell motility in ΔΔ cells. Furthermore, CA c-Src transfected ΔΔ cells displayed even greater motility than WT c-Src transfected ones. This suggests that c-Src activation defect is a major component of ΔΔ cells motility impairment.

Activation of c-Src is dependent on a balance between inhibitory and activating pathways regulating the phosphorylation ratio on Y⁴¹⁶ and Y⁵²⁷ residues (Fig. 6B). Both sides involve several actors, such as kinases and phosphatases [28] as well as adaptor proteins such as DAB1 (Disabled-1) [29]. If integrin signaling is the canonical activation pathway [30], several membrane receptors

Fig. 5 Subcellular localization of phospho FAK, c-Src, and phospho c-Src in WT and $\Delta\Delta$ cells. **A–D** Representative confocal images of pFAK-labeled WT and $\Delta\Delta$ cells. Phospho FAKs were immuno-localized using **A** pY³⁹⁷, **B** pY^{576/577}, **C** pY⁹²⁵, and **D** pY⁸⁶¹ antibodies on fixed cells, labeled with phalloidine-TRITC and DAPI (Green: pFAK, Red: F-actin, Blue: Nuclei). White arrows indicate positive FAs. Areas boxed in yellow are presented in the insets. scale bar = 10 μ m. **E–K** Fluorescent signal quantification: **E, G, I, K** Bar graph of the mean pFAK fluorescence intensity per cell. **F, H, J** Violin plots of the number of pFAK-positive FAs. Quantification was performed on 5 (pY³⁹⁷), 15 (pY^{576/577}), 35 (pY⁹²⁵), and 15 (pY⁸⁶¹) different images for each genotype. For pY⁸⁶¹ FAK, displaying cytoplasmic signal but only a weak signal at FAs, only mean cell fluorescence quantification was conducted. Mean cell fluorescence intensity and/or positive FA number were compared between $\Delta\Delta$ and WT cells. * $p < 0.05$, ** $p < 0.01$, **** $p < 0.0001$ and ns: not significant (Mann–Whitney test). **L–N** Representative confocal images of c-Src, pY⁵²⁷, and pY⁴¹⁶-c-Src-labeled WT and $\Delta\Delta$ cells. c-Src and phospho c-Src were immuno-localized using **L** total c-Src, **M** pY⁵²⁷, **N** pY⁴¹⁶ antibodies on fixed cells, labeled with phalloidine-TRITC and DAPI (Green: c-Src or phospho c-Src, Red: F-actin, Blue: Nuclei). White arrows indicate positive FAs. scale bar = 10 μ m. **O–R** Fluorescent signals quantification: for total c-Src and pY⁵²⁷-c-Src, displaying cytoplasmic signal but only a weak signal at FAs, only mean cell fluorescence quantification was conducted. For pY⁴¹⁶-c-Src, displaying both cytoplasmic signal and intense signal at FAs, mean cell fluorescence intensity and particle analysis were conducted. **O–Q** Histograms of mean c-Src or pY⁵²⁷ or pY⁴¹⁶ signal fluorescence intensity per cell and **R** violin plots of pY⁴¹⁶-c-Src-labeled FAs number were quantified on 20 (c-Src), 10 (pY⁵²⁷) and 30 (pY⁴¹⁶) different images of both WT and $\Delta\Delta$ cells. Mean cell fluorescence intensity and positive FA number were compared between $\Delta\Delta$ and WT. * $p < 0.05$, ** $p < 0.01$, and **** $p < 0.0001$ (Mann–Whitney test). **S** Representative image of western blot analysis of total c-Src and phosphorylated Y⁴¹⁶-c-Src in WT and $\Delta\Delta$ cells. Intensity ratio: ratio of pY⁴¹⁶-c-Src over total c-Src band intensities. **T** Intensity ratio was compared between $\Delta\Delta$ and WT using a Student's *t* test. ** $p < 0.01$.

such as the neurotrophin 3 tyrosine kinase receptor NTRK3, have also been described to activate c-Src [31] (Fig. 6B).

We investigated the pathways regulating c-Src activation by RT-qPCR in $\Delta\Delta$ cells. Interestingly, we observed a strong 7-fold decrease in *Ntrk3* expression associated with a decrease in *Dab1* and an increase in *Ptpn13* transcript levels (Fig. 6C). All of these changes potentially contribute to the decrease in c-Src activation in $\Delta\Delta$ cells.

We then evaluated the relative importance of DAB1, PTPN13, and NTRK3 in $\Delta\Delta$ cell motility defects. Over-expression of DAB1, either its WT form or a phospho-mimetic activated Y185/197D mutant [32], failed to significantly rescue $\Delta\Delta$ cell motility. The same was observed with *Ptpn13* knock-down by CRISPRi (Figs S4C–E), ruling out a major contribution of DAB1 or PTPN13 in $\Delta\Delta$ cell motility defect. We then over-expressed NTRK3 in $\Delta\Delta$ cells and assessed motility. According to RNA-seq data, α T3-1 cells express three NTRK3 isoforms (Fig. 6D): *Ntrk3-201* (Ensembl browser transcript name), the full-length active receptor with both neurotrophin binding and tyrosine kinase (TK) domains, *Ntrk3-205*, an isoform with an additional exon in the TK domain leading to functional deficiency [33] and, finally, the inactive *Ntrk3-202* short variant, without the TK domain. Only expression of the full-length *Ntrk3-201* rescued cell motility in $\Delta\Delta$ cells (Figs. 6D and S4A, B). Interestingly, NTRK3-201 interacts with pY⁴¹⁶-c-Src in α T3-1 cells, as demonstrated by co-immunoprecipitation experiments (Fig. 6E), whereas interactions are noticeably weaker with NTRK3-202 and NTRK3-205 isoforms (2.5-fold reduction compared to NTRK3-201 after normalized quantification). These results suggest that NTRK3 full signaling activity is thus required for c-Src activation. To test whether NTRK3-driven cell motility is dependent on c-Src activity, we measured motility of $\Delta\Delta$ cells expressing NTRK3 alone or together with DN c-Src. We observed that DN c-Src blocks the positive effect of NTRK3 on cell speed (Fig. 6F), indicating that c-Src mediates NTRK3 effect on cell motility.

Altogether, these results demonstrate that immature gonadotrope cell motility is regulated by a Neurod1/4-Ntrk3-Src activation pathway.

NTRK3 regulate gonadotrope cell number and position during mouse pituitary development

To investigate a potential role of *Ntrk3* during gonadotrope differentiation, we first analyzed *Ntrk3-201* transcript levels in the in vitro model of gonadotrope differentiation by RT-qPCR (Fig. 7A). We observed that the active isoform of *Ntrk3* is specifically expressed in α T3-1 cells, representative of E14 to E16 gonadotrope cells.

Gonadotrope cells appear around E13.5 in the mouse developing pituitary, in a restricted ventral area of the *pars distalis* [34]. This population then expands in the pituitary gland and, at E18.5, gonadotrope cells are organized in structured networks throughout the whole anterior lobe of the pituitary

[35]. This expansion during pituitary organogenesis might implicate both proliferation and migration events. To investigate a potential role of *Ntrk3* in gonadotrope cell expansion, we took profit of a *Ntrk3* constitutive knock-out mouse model (*TrkC^{tm1a}*, [36]), and analyzed the gonadotrope cell population in E18.5 *TrkC^{+/-}* (taken as control) and *TrkC^{-/-}* embryos by immunostaining of LH β , a specific marker of gonadotrope cells. We first observed a significant 3-fold decrease in the number of LH β positive cell in *TrkC^{-/-}* embryos as compared to heterozygous controls (Fig. 7B, C), suggesting that NTRK3 might be implicated in pituitary colonization. To test for a regulatory role of NTRK3 on cell motility, we then analyzed the distribution of gonadotrope cells in the pituitary along the antero-posterior and on the dorso-ventral axes. We observed that gonadotrope cells spread significantly less on both axes in *TrkC^{-/-}* fetal pituitaries as compared to *TrkC^{+/-}* (Fig. 7B, D), suggesting that NTRK3 might be implicated in gonadotrope cell migration in vivo.

These results suggest that NTRK3 is an important actor of gonadotrope population organization in the developing pituitary, being implicated in population size as well as in proper colonization of the pituitary anlage.

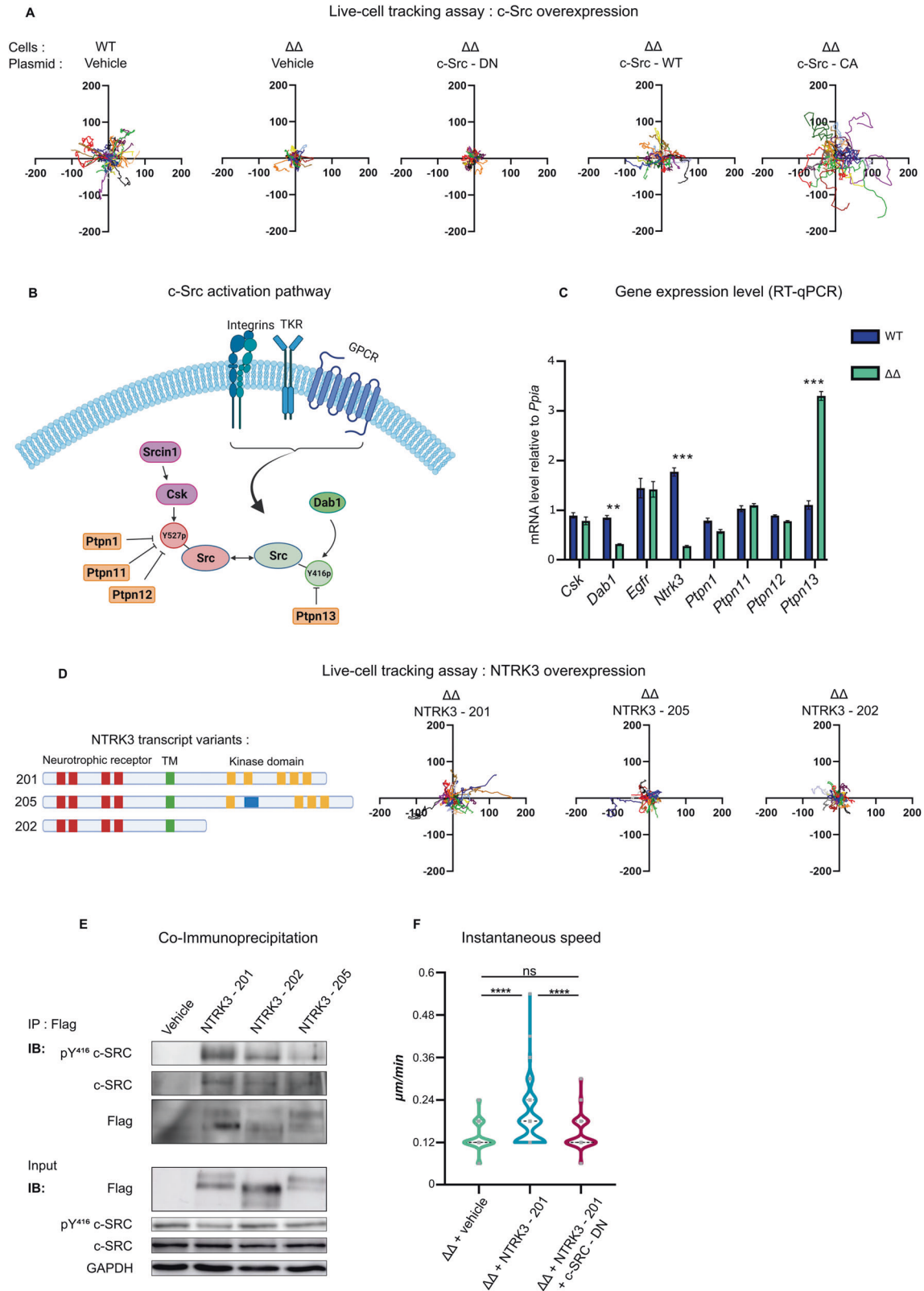
DISCUSSION

The concept of a tridimensional organization of endocrine cell networks in the pituitary gland has only recently emerged [16] and gonadotrope cell networks are now believed to be crucial for proper regulation of reproduction. However, the molecular mechanisms regulating gonadotrope cell motility and, *in fine* the structuration of the endocrine population, remain mostly elusive.

In the current work, we investigated the molecular regulation of gonadotrope cell motility. Using an in silico functional genomic analysis combined with CRISPR/Cas9 cellular knock-out, we demonstrated for the first time that, during pituitary ontogenesis, immature gonadotrope cell motility is regulated by a molecular pathway involving the ND1/4 transcription factors, the neurotrophin NTRK3 receptor and c-Src kinase (Fig. 8A).

In gonadotrope cells, ND1/4 stimulate NTRK3 expression, which in turn interacts with and activates c-Src. Full c-Src kinase activity would be then required for optimal FAK phosphorylation, leading to FA terminal maturation and disassembly. ND1/4 insufficiency, leading to a hypo-activation of c-Src kinase activity, while not affecting its scaffolding role at FAs, unbalances both FAK phosphorylation pattern and FAK distribution, leading to immature FAs accumulation and cell motility defects (Fig. 8B).

Mutation of ND1 and ND4 in gonadotrope cells affects expression of other genes of the c-Src activation pathway such as DAB1 or PTPN13. However, we showed here that, amongst them, only NTRK3



efficiently rescued cell motility, suggesting that, in immature gonadotrope cells, NTRK3 activation of c-Src might be essential to trigger cell motility.

Taking advantage of a knock-out mouse model, we further demonstrated that NTRK3 receptor is crucial to ensure the

colonization of the pituitary gland by gonadotrope cells during embryogenesis. NTRK3 deletion also led to a reduced number of gonadotrope cells that might be explained by a defect in migration, proliferation, or differentiation, in agreement with NTRK3 known functions [37–40].

Fig. 6 $\Delta\Delta$ cells motility defect is rescued by an NTRK3-c-Src signaling pathway. **A** Cell motility rescue assay by c-Src. WT and $\Delta\Delta$ cells were transfected with H2B-mCherry to label and track the nuclei. WT cells were co-transfected with GFP expression plasmid (vehicle) and $\Delta\Delta$ cells were co-transfected with either GFP (vehicle), c-Src DN, c-Src WT, or c-Src CA expression plasmid. Each graph corresponds to 30 representative tracks of transfected WT or $\Delta\Delta$ cells with the initial position of the cells centered at the origin. **B** Schematic representation (created with BioRender) of c-Src inhibition and activation mechanisms. c-Src inhibition involves both Y⁵²⁷ phosphorylation by the CSK kinase and Y⁴¹⁶ dephosphorylation by the PTPN13 phosphatase. Upon extracellular signaling by integrins, c-Src disengages from CSK, with concomitant Y⁵²⁷ dephosphorylation that may involve several putative phosphatases, and finally c-Src autophosphorylates on Y⁴¹⁶. Signal transducing adaptor proteins such as DAB1 (Disabled-1) are known to increase c-Src activation. Finally, membrane receptors such as the neurotrophin 3 tyrosine kinase receptor NTRK3 have also been shown to trigger c-Src activation. **C** Gene expression of the actors of c-Src inhibition and activation pathways in WT and $\Delta\Delta$ cells. Gene expression levels were normalized to *Ppia*. Data are the normalized mean \pm SEM of three independent experiments. Gene expression were compared between $\Delta\Delta$ and WT cells using a Student's *t* test. ns: not significant, ****p* < 0.001. **D** Cell motility rescue assay by NTRK3. (Left) Schematic representation of the *Ntrk3* isoforms expressed in α T3-1 cells. Ligand domain is depicted with red boxes, the transmembrane domain with a green box and the tyrosine kinase domain with yellow boxes. The modified exon in *Ntrk3-205* isoform is represented by a blue box. (Right) Cell motility assay. $\Delta\Delta$ cells were co-transfected with H2B-mCherry and either with *Ntrk3-201*, *Ntrk3-202*, or *Ntrk3-205* isoform expression plasmids. Each graph corresponds to 30 representative tracks of transfected $\Delta\Delta$ cells with the initial position of the cells centered at the origin. **E** c-SRC-NTRK3 co-immunoprecipitation assay. WT cells were co-transfected with c-Src-eGFP and either with 3XFLAG control plasmid (lane 1, vehicle) or 3XFLAG-tagged isoform expression plasmids (Lane 2, *Ntrk3-201*, lane 3 *Ntrk3-202* and lane 4 *Ntrk3-205*). NTRK3 was immunoprecipitated using anti-FLAG M2 antibody-coated magnetic beads. Immuno-precipitates were analyzed by Western blot for NTRK3 precipitation (using anti-FLAG antibody) and for both total and pY⁴¹⁶ c-Src co-precipitations (Top panels). Expression of FLAG-tagged NTRK3, total c-SRC and pY⁴¹⁶ c-SRC-eGFP were verified by western blot analysis on whole cell lysates (Bottom panels). GAPDH was used as an internal reference for sample loading. The different bands observed for NTRK3 isoforms are consistent with glycosylated forms of the receptor. **F** Cell velocity analysis. $\Delta\Delta$ cells were co-transfected with H2B-mCherry and either with GFP (vehicle), *Ntrk3-201*, or a mix of *Ntrk3-201* and DN c-Src expression plasmids. Cell instantaneous speed (μ m/minute) was calculated from the analysis of over 100 transfected $\Delta\Delta$ cells over 16 h videomicroscopy, using ImageJ TrackMate. $\Delta\Delta$ cell mean velocity was compared between the three conditions by ANOVA followed by Tukey multiple comparison test. ns: not significant, ****p* < 0.001.

Because ND1, ND4, and NTRK3 are expressed in other cell types, the Neurod1/4-Ntrk3-Src pathway might also be mobilized in cells requiring motility processes throughout their differentiation. For example, this pathway is expressed in human testicular spermatids according to the human protein atlas database and, although spermatid motility is an important part of their differentiation [41], the underlying molecular mechanisms are still poorly understood.

Whereas both ND1 and NTRK3 have already been reported to regulate cell motility [39, 42–45], much less was known about ND4 cellular function. We showed here that ND4 is as potent as ND1 to regulate gonadotrope cell motility. The transcriptional activity of ND4 would, however, be more important than ND1 for gonadotrope cells since ND1 only partially compensates for ND4 absence.

Pituitary gonadotrope cells display a remarkable functional plasticity during adulthood, which is essential to regulate fertility. Gonadotrope cell networks are suspected to play a important role in this plasticity as they are reconfigured under physiological challenges such as puberty and lactation [46]. However, little is known about the regulation of gonadotrope cell motility [47, 48] or migratory ability [49] during these events. Interestingly NTRK3 remains expressed in adult gonadotrope cells, as demonstrated by single-cell transcriptomic analysis of adult rat pituitaries [50]. NTRK3, which has recently been implicated in neural network formation [51], could thus be a major actor of gonadotrope cell network plasticity during reproductive life. It would be thus interesting to analyze NTRK3 signaling in adult pituitary during critical physiological demands.

Dysregulations of NTRK3 signaling are known to be implicated in numerous cancers [52]. Gonadotrope adenomas are frequent cancers accounting for approximately 40% of all pituitary adenomas [53, 54]. However, most gonadotrope adenomas are poorly characterized and the molecular etiology of gonadotrope cell carcinogenesis is mostly unknown. A screen of NTRK3 mutations in these cancers should open new therapeutic avenues.

In conclusion, our work provides new insights into the molecular pathways controlling gonadotrope cell positioning during their differentiation in the developing pituitary and should contribute to a better understanding of the role of gonadotrope cell networks. Further studies are needed to establish whether this pathway is also mobilized at adulthood and contributes to the adaptation of gonadotrope cell population to physiological challenges at the critical stages of the reproductive life.

MATERIALS AND METHODS

Materials

Primary and secondary antibodies along with primers used for RT-qPCR, PCR genotyping, *cis*-regulatory regions, gRNAs, and ORFs cloning are described in supplementary table 2.

Cell cultures

The α T1-1, α T3-1, and L β T2 mouse gonadotrope cell lines (generously given by P. Mellon, University of California, La Jolla, CA) were grown in high-glucose DMEM supplemented with 10% fetal bovine serum (FBS from Gibco) and 0.1% penicillin/streptomycin, at 37 °C with 5% CO₂. Cells are regularly tested for mycoplasma and for proper cell identity.

In silico analysis

NEURD01 ChIP-seq Bed files (GSM3579940 [8] and GSM1306336 [55]) were retrieved from the ChIP-atlas website [22] and cross-referenced for overlapping target regions with the α T3-1 ATAC-seq [20] using bedtools intersect [56]. Only NEURD01 ChIP-seq data were used as there is no available ChIP-seq data for NEURD04 in the mouse. Genomic regions were then associated with the nearest gene Transcription Start Site using Homer annotatePeaks.pl [57]. Pathway analysis and network clustering were performed using Cytoscape ClueGO software [23].

RNA extraction and mRNA quantification

Total cellular RNAs were isolated using *TRIzol*TM Reagent according to the manufacturer's protocol. RNAs (2 μ g) were reverse transcribed with SuperScript II reverse transcriptase (ThermoFisher Scientific) using random primers according to the manufacturer's instructions. qPCR quantifications were performed using TakyonTM 2X MasterMix from Eurogentec. Experiments were conducted independently in at least 3 replicates.

Immunocytofluorescence

Cells were seeded at a density of 500 cells/mm² on Nunc[®] Lab-Tek[®]. Coating was performed using Corning[®] Matrigel[®] Growth Factor Reduced (GFR) basement membrane matrix diluted in PBS (1/50) for 30 min at 37 °C. Cells were fixed 48 h after plating, with 4% PFA for 15 min, and 0.1% Triton X-100 permeabilization was performed. Permeabilized cells were then incubated with primary antibodies overnight at 4 °C and then with Alexa488 secondary antibodies 1 h at room temperature (RT). F-actin was labeled using Rhodamin-Phalloidin (ThermoFisher Scientific) and nuclei were labeled using DAPI.

Images were acquired using the ZEISS LSM 700 confocal microscope on the Functional and Adaptive Biology Unit microscopy facility, using laser settings and digital gain as described for each antibody in the additional file 2.

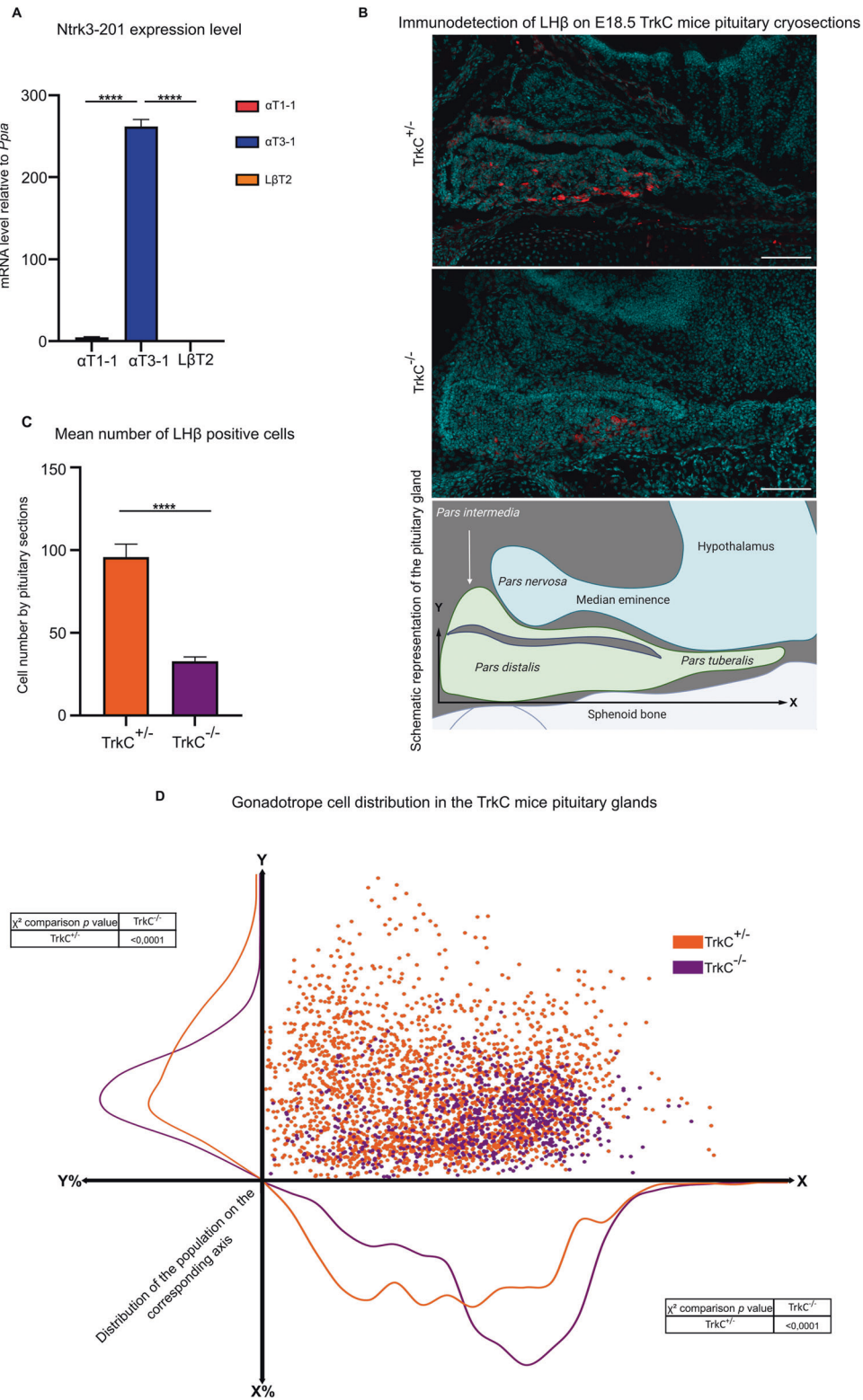


Image analyses

Images were analyzed using the ImageJ software [58]. For each image, cell number was assessed by counting the number of DAPI positive nuclei.

According to the signal patterns, we either quantified total intensity of fluorescence and/or FA number by particle analysis. Intensity of fluorescence

was quantified using the “measure” option of the ImageJ software, after setting a minimum threshold value of 5 for each image. Raw Intensity values obtained were then compared to the number of nucleus per image to assess an approximated value of intensity for each cell type. Mean cell surface was assessed using the “measure” option of the ImageJ software, after setting a minimum threshold value of 5 for each image. Area values obtained were

Fig. 7 NTRK3 regulates gonadotrope cell positioning in the developing pituitary in vivo. **A** *Ntrk3* active isoform expression in the in vitro model of gonadotrope differentiation. *Ntrk3-201* expression level was quantified by qPCR and normalized to *Ppia*. Data are the normalized mean \pm SEM of three independent experiments. *Ntrk3-201* expression level was compared to α T3-1 cells using an ANOVA followed by Dunnett's multiple comparison test. **** $p < 0.0001$. **B** Gonadotrope cell population distribution in TrkC mouse embryonic pituitary at E18.5. LH beta sub-unit (LH β), specifically expressed by gonadotrope cells, was detected by immunohistofluorescence on E18.5 TrkC $^{+/-}$ and TrkC $^{-/-}$ embryo cryosections. Nuclei were stained by DAPI. Top and middle panels: Representative images of TrkC $^{+/-}$ (taken as control) and TrkC $^{-/-}$ pituitary sections. scale bar = 100 μ m. Bottom panel: schematic representation of the pituitary and surrounding structures at E18.5. The pituitary gland sits between the palate sphenoid bone (ventral) and the *pars nervosa* and median eminence (dorsal). Gonadotrope cells, labeled in red, are mostly localized in the *pars distalis*, the ventral part of the endocrine pituitary. X and Y black arrows: cartesian coordinate system used to analyze gonadotrope cell distributions. **C** Quantification of gonadotrope cell number in TrkC $^{+/-}$ and TrkC $^{-/-}$ embryonic pituitary at E18.5. LH β -expressing gonadotrope cells were enumerated on a minimum of six sections of three female individuals for each genotype. Histological sections were matched between genotypes for similar anatomical positions. Only sections with complete pituitary of the same surface, and containing both *pars nervosa* and median eminence were retained to minimize counting bias. Number of gonadotrope cells per sections were compared between genotypes. **** $p < 0.0001$ (Mann–Whitney test). **D** Distribution of the gonadotrope cell population within the pituitary of TrkC $^{+/-}$ and TrkC $^{-/-}$ embryos at E18.5 (Green; TrkC $^{+/-}$ and red: TrkC $^{-/-}$). Each identified gonadotrope cell on each section was plotted on a standardized cartesian coordinate (X;Y) system with the antero-posterior embryo axis represented by "X" and the dorso-ventral axis by "Y". For each genotype, histograms of gonadotrope cell distributions on both X and Y axis were estimated. Distribution on each axis were compared using χ^2 comparison test.

then normalized to the number of nucleus per image to evaluate the approximated surface covered by each cell type. Particle quantification was performed using the ImageJ software by reducing background for both actin and immuno-labeled protein signals with a Rolling ball radius of 2.5 pixels. Then, threshold of the immuno-labeled protein channel was set using the "Auto Local Threshold" tool with the "Phansalkar" method (radius of 25 and specific parameters value of 0.1). Actin and immuno-labeled protein colocalization was then assessed using the "Colocalization Threshold" tool. Colocalizing particles were analyzed with the "Analyze Particles" tool using the following parameters: "size: 0.3 pixel² – infinity" "circularity: 0.0–0.8". The number of particles counted was then normalized to the number of nuclei within each image.

Particle analysis for FAK pY³⁹⁷ and FAK pY⁹²⁵, displaying a high signal to background ratio at FA, was performed using the Analyze Particles command directly on the immuno-labeled protein channel without prior actin colocalization. Only objects with size ranging from 0.2 to 5 pixel² and circularity parameter ranging from 0.0 to 0.7 were considered. Finally, the total count of particles for each image was normalized to the nucleus number.

Luciferase reporter assay

Cloning of the potential *cis*-regulatory regions of *Neurod4*: potential *cis*-regulatory element genomic regions were amplified from mouse DNA. *Neurod4* proximal promoter (R2 region) was cloned upstream the luciferase gene in the pGL4.12 backbone (Promega). R1, R3, R4, R5, and R6 potential enhancers were then cloned in the pR2-GL4 vector downstream the SV40 poly(A) signal, between the BamHI and Sall sites. Cell transfection was performed as follows: briefly, 50,000 cells were transiently transfected in 96-well plates using Lipofectamine[®] 3000 (ThermoFisher Scientific) with 100 ng/well of pGL4 plasmids along with 5 ng/well of pRL-SV Renilla plasmid as an internal control for normalization. After 48 h transfection, firefly and Renilla luciferase activities were measured using the Dual-Luciferase Reporter Assay System (Promega). Each experiment was performed six times independently in triplicates. Data were normalized to Renilla for each condition. ANOVA followed by Dunnett's multiple comparison test was performed independently for each cell line and condition.

CRISPR/Cas9 deletions of *Neurod1* and *Neurod4* R6 region

pLV hUbc-Cas9-T2A-GFP (#53190), and pSPgRNA (#47108) plasmids [59] were purchased from Addgene. Specific guide RNAs, on both side of *Neurod1* ORF or *Neurod4* R6 enhancer, were designed using CCTop online tool [60] and cloned in pSPgRNA plasmid.

About 5×10^6 α T3-1 cells were electroporated with the Cas9 expression vector and the gRNA couples expression plasmids at a ratio of 1.5:8.5 μ g using a Neon[™] Transfection System (Invitrogen) according to the manufacturer's protocol (two pulses at 1500 mV for 15 ms). The empty pSPgRNA was used as control. After 48 h, GFP-positive cells were sorted using the FACS Aria II on the PIC2 facility of the Unit of Functional and Adaptive Biology. Sorted cells were then plated at low density until colonies were formed. Δ ND1 and Δ ND4 singles colonies were then genotyped for the *Neurod1* locus and for the *Neurod4* R6 region, respectively, using primers described in additional file 2. To generate *Neurod1* and *Neurod4* $\Delta\Delta$ mutants, the R6 enhancer was deleted in a Δ ND1 α T3-1 clone following the same protocol.

Protein extraction and western blot

Cellular proteins were extracted using a modified RIPA lysis buffer (150 mM NaCl; 50 mM Tris pH 8; 1% Triton X-100; 0.1% SDS; 1/1000 DNase, supplemented with 1/100 Phosphatase and protease inhibitor cocktail from ThermoFisher Scientific) and separated on a 10% SDS-PAGE. After transfer, nitrocellulose membranes were incubated overnight at 4 °C with primary antibodies against Src and pY⁴¹⁶Src diluted in Tris-buffered saline containing 0.01% Tween 20 (TBS-T) supplemented with 5% milk. After extensive washing, blots were incubated with a horseradish peroxidase-conjugated secondary antibody (GE healthcare #NA934V) in TBS-T/5% milk for 60 min at RT and then washed. Immunodetection was performed using an enhanced chemiluminescence detection system (GE Healthcare). Uncropped western blot images are shown in supplementary data.

ORFs cloning

For rescue experiments, the pIRES-hyg3 backbone (Clontech) was modified to express a 2A-GFP cassette. *c-Src*, *Dab1*, and *Ntrk3* isoforms coding sequences were amplified from α T3-1 cDNAs and inserted in frame in the p2A-GFP IRES hyg3 backbone. Constitutively activated (CA) and Dominant Negative (DN) *c-Src* and phospho-mimetic DAB1 were obtained by fusion PCR mutagenesis.

WT *c-Src* was further subcloned in pEGFP N1 backbone in frame with GFP (pSrc-eGFP). A 3X FLAG tag was inserted in Cter of each *Ntrk3* isoforms (pNtrk3-3XFLAG 201, 202 and 205).

Motility assay

Cells were transfected by electroporation with pH2B-mCherry to track nucleus position (0.5×10^6 cells, 1 μ g plasmid, two pulses at 1500 mV for 15 ms). For *c-Src*, *Ntrk3*, and *Dab1* rescue experiments, cells were co-transfected with *c-Src*, *Ntrk3*, or *Dab1* expression plasmids. For *Ptpn13* knockdown, cells were co-transfected with a pLV hUbc-Zim3KRAB hdCas9-T2A-GFP, expressing a dead Cas9 (Addgene #53191) fused with the repressor KRAB domain of the human ZIM3 gene (as described in [61]), and gRNA targeting *Ptpn13* proximal promoter described in [62] and supplementary table 2). Cells were then seeded in 12-well plates coated with 1/50^e Corning[®] Matrigel[®] GFR at a density of 25,000 cells/cm². mCherry fluorescent nuclei were then followed using video time-lapse microscopy at 37 °C and 5% CO₂ during 16 h. Cell displacement analysis and tracking were done on the red channel using the ImageJ software with the "TrackMate" plugin, using the following parameters: LoG detector, threshold of 3.0, the HyperStack Displayer, Simple LAP tracker, 75 microns Gap-closing max distance, 15 microns linking max distance and 5 microns Gap-closing max frame gap. Only cells displaying red nuclei signal, green cytoplasmic signal and directly adhering to the matrix through the whole movie were kept for analysis.

FluoroBlock cell migration assay

150,000 cells/cm² were seeded in the top part of Corning[®] FluoroBlok[™] Cell Culture Inserts in DMEM serum-deprived medium for 24 h. Medium in the bottom chamber was then replaced by 10% FBS DMEM medium to induce cell migration. After 16 h, cells were labeled with the fluorescent Calcein

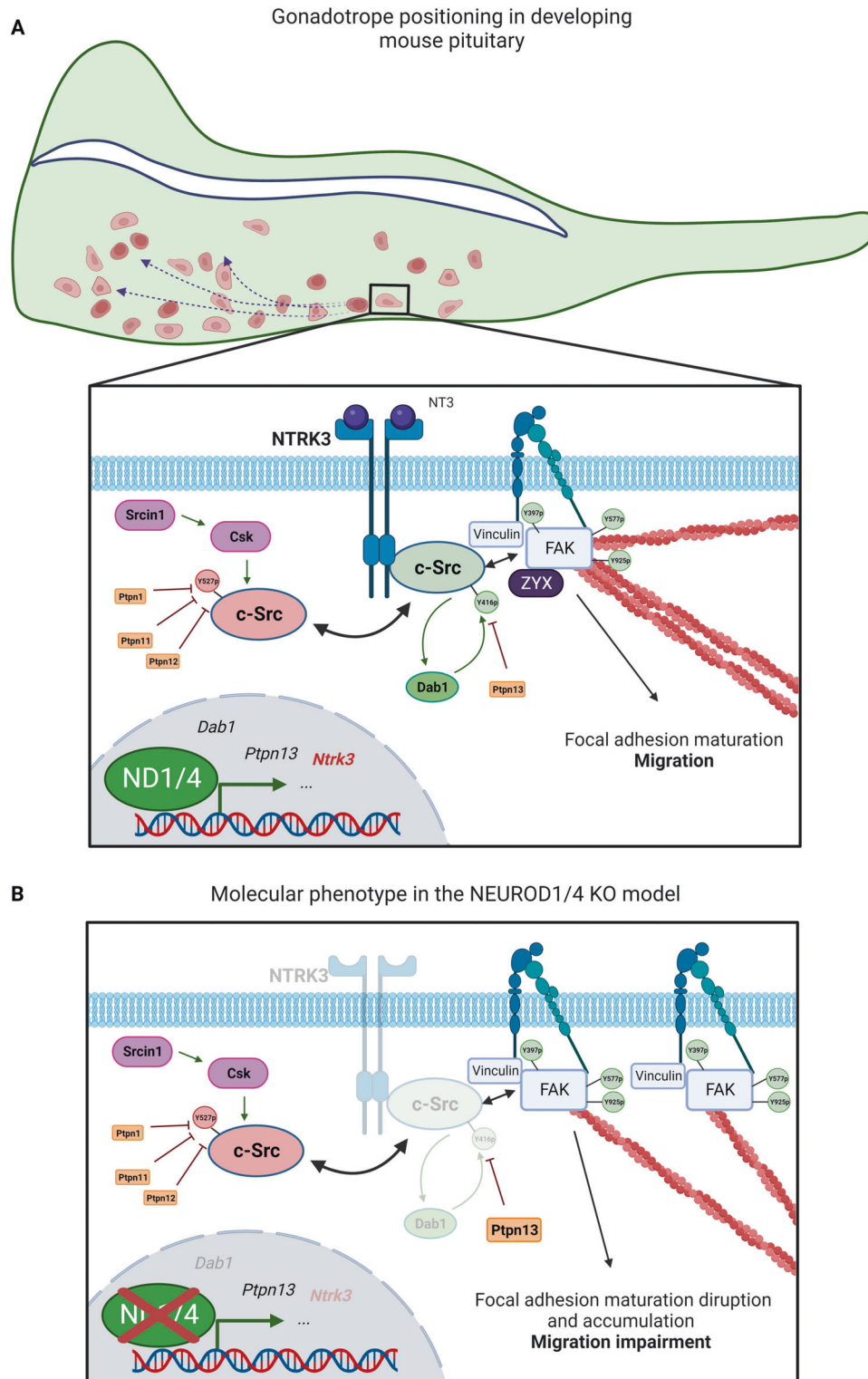


Fig. 8 The Neurod1/4-Ntrk3-Src pathway regulates gonadotrope cell motility during gonadotrope differentiation. Schematic representation of the principal results of this study (created with BioRender). **A** Gonadotrope cells (in red) differentiate in the ventral part of the pituitary and then disseminate in the gland. Our work shows that gonadotrope cell motility during pituitary organogenesis is dependent on NTRK3 receptor whose expression is controlled by ND1 and ND4 transcription factors. NTRK3 interacts with c-Src kinase and promotes its activation, a prerequisite for maturation of FAs and cell migration. **B** NEUROD1/4 insufficiency leads to a defect in NTRK3 expression, leading to a c-Src hypo-activation, which, in turn, disturbs FAK phosphorylation pattern. These signaling disruptions induce an accumulation of immature focal adhesions, preventing cell migration.

AM dye (ThermoFisher Scientific) in Hank's Balanced Salt Solution for 2 h. Bottom Fluorescence intensity, corresponding to post-migratory cells was measured using a FlexStation3 microplate reader at λ 495 nm.

Cell adhesion assay

WT and $\Delta\Delta$ cells were labeled with Calcein AM dye in Hank's Balanced Salt Solution for 30 min. Labeled cells were seeded on an uncoated cell surface of 96-well transparent bottom plate for 30 min. Initial bottom fluorescence was read using a FlexStation3 microplate reader at λ 495 nm and then cells were flushed away by two PBS washes. Residual bottom fluorescence was then read and the relative number of attached cells was estimated by calculating the percentage of remaining fluorescence intensity.

Co-immunoprecipitation

15×10^6 WT α T3-1 cells were co-transfected with c-SRC-eGFP and NTRK3 isoform expression plasmids (pNtrk3-3XFLAG 201, 202 and 205) by electroporation for 24 h. Cellular proteins were extracted using a modified RIPA lysis buffer (150 mM NaCl; 50 mM Tris pH 8; 1% Triton X-100 containing 1/100 Phosphatase and protease inhibitor cocktail). Extracts were incubated overnight with anti-FLAG M2 antibody (F1804, Sigma-Aldrich) and then with Dynabeads™ Proteine G (ThermoFisher Scientific) for 4 h. Beads were then extensively washed in modified RIPA lysis buffer and eluted with Laemmli buffer. Eluted proteins were then immunodetected for pY⁴¹⁶c-Src by western blot. Input protein extracts were immunoblotted for NTRK3 (FLAG), pY⁴¹⁶c-Src, c-Src, and GAPDH). The ImageJ software was used for band intensity quantification. Uncropped western blot images are shown in supplementary data.

Immunohistofluorescence

The TrkC^{tm1a} is a mouse gene-trap model with a trapping cassette located in between the 4th and 5th exons of Ntrk3 gene, resulting in a full Ntrk3 knock-out model. This model is hosted in the controlled environment of the animal facility (P-PAC) in the Cancer Research Center of Lyon, with ad libitum feeding (French Ministry for Research, registered number C2EA15, protocol CECCAPP CLB_2010_22). TrkC^{tm1a} E18.5 embryos were obtained by crossing TrkC^{+/-} mice. TrkC^{tm1a} E18.5 embryos were obtained by crossing TrkC^{+/-} mice. Pregnant mice were killed by cervical dislocation. Embryos were retrieved and fixated in PBS containing 4% PFA for 24 h. Fixed embryos were incubated in 30% sucrose and then embedded in OCT media (Cellpath, Newtown, UK), before being frozen at -80°C . Embryos were PCR sexed using the mRbm31xy primers (described in [63]) and genotyped for Ntrk3 KO using the Lar primers [36] (Supplementary table 2). Female embryos were cryosectioned (15 μm thickness cuts). Cryosections were post-fixed in PBS-PFA 4% for 15 min, blocked with 10% Goat serum diluted in PBS for 1 h and then incubated overnight at 4°C with anti-LH β antibody (gift of Dr J.F. Roser, University of California Davis, USA). In vitro generated Alexa Fluor antibodies were used as secondary antibodies. Nuclei were stained with DAPI and slides were mounted in ProLong Gold Antifade Mountant (ThermoFisher Scientific) for imaging. Images were acquired using the ZEISS LSM 700 confocal microscope on the Functional and Adaptive Biology Unit microscopy facility. For each genotype, at least 6 different pituitary sections of 3 embryos were studied. To reduce position bias, images were taken at standardized anatomical positions. Only images with complete pituitary glands of similar total area along with *pars nervosa* and median eminence were kept for analysis. More than 800 LH β positive cells were counted per genotype. To compare cell distributions between genotypes, gonadotrope cell positions were plotted on a Cartesian coordinate system with an origin point fixed at the ventro-posterior tips of the *pars distalis* (schematic representation, Fig. 7B). Cell histogram distributions were plotted on both the X and Y axis and compared between genotypes using χ^2 comparison test.

Statistical analysis

Analyses were performed in double-blinded experimental setups. Statistical analyses were performed using the Prism-GraphPad software. Test types and parameters are detailed in each figure legend.

Representative image adjustment

Maximum displayed value of signal (ImageJ software) were linearly adjusted using identical parameters between test and control conditions.

DATA AVAILABILITY

The GSM3579940 and GSM1306336 NEURD01 ChIP-seq raw data Bed files are available in the ChIP-atlas (<https://chip-atlas.org/>) repository. The GSE104513 α T3-1 RNA-seq dataset is available in the Gene Expression Omnibus repository and the α T3-1 ATAC-seq dataset is accessible upon reasonable request.

REFERENCES

- Tutukova S, Tarabykin V, Hernandez-Miranda LR. The role of neurod genes in brain development, function, and disease. *Front Mol Neurosci*. 2021;14:662774.
- Dennis DJ, Han S, Schuurmans C. bHLH transcription factors in neural development, disease, and reprogramming. *Brain Res*. 2019;1705:48–65.
- Bertrand N, Castro DS, Guillemot F. Proneural genes and the specification of neural cell types. *Nat Rev Neurosci*. 2002;3:517–30.
- Cho JH, Klein WH, Tsai MJ. Compensational regulation of bHLH transcription factors in the postnatal development of BETA2/NeuroD1-null retina. *Mech Dev*. 2007;124:543–50.
- Cherry TJ, Wang S, Bormuth I, Schwab M, Olson J, Cepko CL. NeuroD factors regulate cell fate and neurite stratification in the developing retina. *J Neurosci*. 2011;31:7365–79.
- Gu C, Stein GH, Pan N, Goebbels S, Hörnberg H, Nave KA, et al. Pancreatic beta cells require NeuroD to achieve and maintain functional maturity. *Cell Metab*. 2010;11:298–310.
- Li HJ, Ray SK, Pan N, Haigh J, Fritsch B, Leiter AB. Intestinal NeuroD1 expression impairs paneth cell differentiation and promotes enteroendocrine lineage specification. *Sci Rep*. 2019;9:19489.
- Poulin G, Lebel M, Chamberland M, Paradis FW, Drouin J. Specific protein-protein interaction between basic helix-loop-helix transcription factors and homeoproteins of the Pitx family. *Mol Cell Biol*. 2000;20:4826–37.
- Liu J, Lin C, Gleiberman A, Ohgi KA, Herman T, Huang HP, et al. Tbx19, a tissue-selective regulator of POMC gene expression. *Proc Natl Acad Sci USA*. 2001;98:8674–9.
- Zhu X, Zhang J, Tollkühn J, Ohsawa R, Bresnick EH, Guillemot F, et al. Sustained Notch signaling in progenitors is required for sequential emergence of distinct cell lineages during organogenesis. *Genes Dev*. 2006;20:2739–53.
- Kouki T, Imai H, Aoto K, Eto K, Shioda S, Kawamura K, et al. Developmental origin of the rat adenohypophysis prior to the formation of Rathke's pouch. *Development* 2001;128:959–63.
- Sánchez-Arrones L, Ferrán JL, Hidalgo-Sánchez M, Puelles L. Origin and early development of the chicken adenohypophysis. *Front Neuroanat*. 2015;9:7.
- Schlosser G. Induction and specification of cranial placodes. *Dev Biol*. 2006;294:303–51.
- Ward RD, Raetzman LT, Suh H, Stone BM, Nasonkin IO, Camper SA. Role of PROP1 in pituitary gland growth. *Mol Endocrinol*. 2005;19:698–710.
- Zhu X, Gleiberman AS, Rosenfeld MG. Molecular physiology of pituitary development: signaling and transcriptional networks. *Physiol Rev*. 2007;87:933–63.
- Mollard P, Hodson DJ, Lafont C, Rizzotti K, Drouin J. A tridimensional view of pituitary development and function. *Trends Endocrinol Metab*. 2012;23:261–9.
- Lamolet B, Poulin G, Chu K, Guillemot F, Tsai MJ, Drouin J. Tpit-independent function of NeuroD1(BETA2) in pituitary corticotroph differentiation. *Mol Endocrinol*. 2004;18:995–1003.
- Ando M, Goto M, Hojo M, Kita A, Kitagawa M, Ohtsuka T, et al. The proneural bHLH genes Mash1, Math3 and NeuroD are required for pituitary development. *J Mol Endocrinol*. 2018;61:127–38.
- Alarid ET, Windle JJ, Whyte DB, Mellon PL. Immortalization of pituitary cells at discrete stages of development by directed oncogenesis in transgenic mice. *Development* 1996;122:3319–29.
- Xie H, Hoffmann HM, Iyer AK, Brayman MJ, Ngo C, Sunshine MJ, et al. Chromatin status and transcription factor binding to gonadotropin promoters in gonadotrope cell lines. *Reprod Biol Endocrinol*. 2017;15:86.
- Pacini V, Petit F, Querat B, Laverrière JN, Cohen-Tannoudji J, L'hôte D. Identification of a pituitary ER α -activated enhancer triggering the expression of Nr5a1, the earliest gonadotrope lineage-specific transcription factor. *Epigenetics Chromatin*. 2019;12:48.
- Zou Z, Ohta T, Miura F, Oki S. ChIP-Atlas 2021 update: a data-mining suite for exploring epigenomic landscapes by fully integrating ChIP-seq, ATAC-seq and Bisulfite-seq data. *Nucleic Acids Res*. 2022;50:W175–182.
- Bindea G, Mlecnik B, Hackl H, Charoentong P, Tosolini M, Kirilovsky A, et al. ClueGO: a Cytoscape plug-in to decipher functionally grouped gene ontology and pathway annotation networks. *Bioinformatics* 2009;25:1091–3.

24. Zaidel-Bar R, Ballestrem C, Kam Z, Geiger B. Early molecular events in the assembly of matrix adhesions at the leading edge of migrating cells. *J Cell Sci*. 2003;116:4605–13.
25. Mitra SK, Schlaepfer DD. Integrin-regulated FAK-Src signaling in normal and cancer cells. *Curr Opin Cell Biol*. 2006;18:516–23.
26. Brunton VG, Avizienyte E, Fincham VJ, Serrels B, Metcalf CA, Sawyer TK, et al. Identification of Src-specific phosphorylation site on focal adhesion kinase: dissection of the role of Src SH2 and catalytic functions and their consequences for tumor cell behavior. *Cancer Res*. 2005;65:1335–42.
27. Deramaudt TB, Dujardin D, Hamadi A, Noulet F, Kolli K, De Mey J, et al. FAK phosphorylation at Tyr-925 regulates cross-talk between focal adhesion turnover and cell protrusion. *Mol Biol Cell*. 2011;22:964–75.
28. Roskoski R. Src kinase regulation by phosphorylation and dephosphorylation. *Biochem Biophys Res Commun*. 2005;331:1–14.
29. Bock HH, Herz J. Reelin activates SRC family tyrosine kinases in neurons. *Curr Biol*. 2003;13:18–26.
30. Huvencsers S, Danen EHJ. The interaction of SRC kinase with beta3 integrin tails: a potential therapeutic target in thrombosis and cancer. *ScientificWorldJournal*. 2010;10:1100–5.
31. Jin W, Yun C, Hobbie A, Martin MJ, Sorensen PHB, Kim SJ. Cellular transformation and activation of the phosphoinositide-3-kinase-Akt cascade by the ETV6-NTRK3 chimeric tyrosine kinase requires c-Src. *Cancer Res*. 2007;67:3192–200.
32. Feng L, Cooper JA. Dual functions of Dab1 during brain development. *Mol Cell Biol*. 2009;29:324–32.
33. Valenzuela DM, Maisonnier PC, Glass DJ, Rojas E, Nuñez L, Kong Y, et al. Alternative forms of rat TrkC with different functional capabilities. *Neuron*. 1993;10:963–74.
34. Granger A, Ngô-Muller V, Bleux C, Guigon C, Pincas H, Magre S, et al. The promoter of the rat gonadotropin-releasing hormone receptor gene directs the expression of the human placental alkaline phosphatase reporter gene in gonadotrope cells in the anterior pituitary gland as well as in multiple extra-pituitary tissues. *Endocrinology*. 2004;145:983–93.
35. Budry L, Lafont C, El Yandouzi T, Chauvet N, Conéjero G, Drouin J, et al. Related pituitary cell lineages develop into interdigitated 3D cell networks. *Proc Natl Acad Sci USA*. 2011;108:12515–20.
36. Ménard M, Costechareyre C, Coelho-Aguiar JM, Jarrosson-Wuillaume L, Rama N, Blachier J, et al. The dependence receptor TrkC regulates the number of sensory neurons during DRG development. *Dev Biol*. 2018;442:249–61.
37. Cui Y, Yin Y, Zou Y, Zhao Y, Han J, Xu B, et al. The Rotary Cell Culture System increases NTRK3 expression and promotes neuronal differentiation and migratory ability of neural stem cells cultured on collagen sponge. *Stem Cell Res Ther*. 2021;12:298.
38. Bové M, Monto F, Guillem-Llobat P, Ivorra MD, Noguera MA, Zambrano A, et al. NT3/TrkC pathway modulates the expression of UCP-1 and adipocyte size in human and rodent adipose tissue. *Front Endocrinol*. 2021;12:630097.
39. Zanin JP, Battiatto NL, Rovasio RA. Neurotrophic factor NT-3 displays a non-canonical cell guidance signaling function for cephalic neural crest cells. *Eur J Cell Biol*. 2013;92:264–79.
40. Bartkowska K, Paquin A, Gauthier AS, Kaplan DR, Miller FD. Trk signaling regulates neural precursor cell proliferation and differentiation during cortical development. *Development*. 2007;134:4369–80.
41. Qian X, Mruk DD, Cheng YH, Tang EI, Han D, Lee WM, et al. Actin binding proteins, spermatid transport and spermiation. *Semin Cell Dev Biol*. 2014;30:75–85.
42. Singh SP, Wolfe A, Ng Y, DiVall SA, Buggs C, Levine JE, et al. Impaired estrogen feedback and infertility in female mice with pituitary-specific deletion of estrogen receptor alpha (ESR1). *Biol Reprod*. 2009;81:488–96.
43. Ikematsu Y, Tanaka K, Toyokawa G, Ijichi K, Ando N, Yoneshima Y, et al. NEUROD1 is highly expressed in extensive-disease small cell lung cancer and promotes tumor cell migration. *Lung Cancer*. 2020;146:97–104.
44. Ivanov SV, Panaccione A, Brown B, Guo Y, Moskaluk CA, Wick MJ, et al. TrkC signaling is activated in adenoid cystic carcinoma and requires NT-3 to stimulate invasive behavior. *Oncogene*. 2013;32:3698–710.
45. Kim WY. NeuroD regulates neuronal migration. *Mol Cells*. 2013;35:444–9.
46. Alim Z, Hartshorn C, Mai O, Stitt I, Clay C, Tobet S, et al. Gonadotrope plasticity at cellular and population levels. *Endocrinology*. 2012;153:4729–39.
47. Gronlien HK, Fontaine R, Hodne K, Tysseng I, Ager-Wick E, Weltzien FA, et al. Long extensions with varicosity-like structures in gonadotrope Lh cells facilitate clustering in medaka pituitary culture. *PLoS ONE*. 2021;16:e0245462.
48. Rahamim-Ben Navi L, Tsukerman A, Feldman A, Melamed P, Tomić M, Stojilkovic SS, et al. GnRH induces ERK-dependent bleb formation in gonadotrope cells, involving recruitment of members of a GnRH receptor-associated signalosome to the blebs. *Front Endocrinol (Lausanne)*. 2017;8:113.
49. Godoy J, Nishimura M, Webster NJG. Gonadotropin-releasing hormone induces miR-132 and miR-212 to regulate cellular morphology and migration in immortalized LbetaT2 pituitary gonadotrope cells. *Mol Endocrinol*. 2011;25:810–20.
50. Fletcher PA, Smiljanic K, Maso Prévêde R, Iben JR, Li T, Rokic MB, et al. Cell type- and sex-dependent transcriptome profiles of rat anterior pituitary cells. *Front Endocrinol*. 2019;10:623.
51. Li G, Zhang B, Sun JH, Shi LY, Huang MY, Huang LJ, et al. An NT-3-releasing bioscaffold supports the formation of TrkC-modified neural stem cell-derived neural network tissue with efficacy in repairing spinal cord injury. *Bioact Mater*. 2021;6:3766–81.
52. Manea CA, Badiu DC, Ploscaru IC, Zgura A, Bacinschi X, Smarandache CG, et al. A review of NTRK fusions in cancer. *Ann Med Surg*. 2022;79:103893.
53. Asa SL, Ezzat S. Gonadotrope tumors. *Prog Mol Biol Transl Sci*. 2016;143:187–210.
54. Ntali G, Capatina C. Updating the landscape for functioning gonadotroph tumors. *Medicina*. 2022;58:1071.
55. Jia S, Ivanov A, Blasevic D, Müller T, Purfürst B, Sun W, et al. Insm1 cooperates with NeuroD1 and Foxa2 to maintain mature pancreatic β -cell function. *EMBO J*. 2015;34:1417–33.
56. Quinlan AR, Hall IM. BEDTools: a flexible suite of utilities for comparing genomic features. *Bioinformatics*. 2010;26:841–2.
57. Heinz S, Benner C, Spann N, Bertolino E, Lin YC, Laslo P, et al. Simple combinations of lineage-determining transcription factors prime cis-regulatory elements required for macrophage and B cell identities. *Mol Cell*. 2010;38:576–89.
58. Schindelin J, Arganda-Carreras I, Frise E, Kaynig V, Longair M, Pietzsch T, et al. Fiji: an open-source platform for biological-image analysis. *Nat Methods*. 2012;9:676–82.
59. Kabadi AM, Ousterout DG, Hilton IB, Gersbach CA. Multiplex CRISPR/Cas9-based genome engineering from a single lentiviral vector. *Nucleic Acids Res*. 2014;42:e147.
60. Stemmer M, Thumberger T, Keyer M, del S, Wittbrodt J, Mateo JL. CCTop: an intuitive, flexible and reliable CRISPR/Cas9 target prediction tool. *PLoS ONE*. 2015;10:e0124633.
61. Alerasool N, Segal D, Lee H, Taipale M. An efficient KRAB domain for CRISPRi applications in human cells. *Nat Methods*. 2020;17:1093–6.
62. Horlbeck MA, Gilbert LA, Villalta JE, Adamson B, Pak RA, Chen Y, et al. Compact and highly active next-generation libraries for CRISPR-mediated gene repression and activation. *Elife*. 2016;5:e19760.
63. Tunster SJ. Genetic sex determination of mice by simplex PCR. *Biol Sex Differ*. 2017;8:31.

ACKNOWLEDGEMENTS

This work benefited from equipment and services from the PIC2 facility and the imaging facilities from both the Unit of Functional and Adaptive Biology and the ImagoSeine core facility, the latter being a member of the France Biolmaging infrastructure supported by grant ANR-10-INBS-04 from the French National Research Agency. We are thankful to Stefania Tolu for her help with the FACS experiments. We also thank Dr Pamela Mellon who developed and provided us with the gonadotrope cell lines. We are very grateful to Patrick Mehlen who generously gave us access to the TrkC^{tm1a} mouse model. We also would like to thank numerous generous colleagues for their gifts of several of the antibodies used in this work, namely Dr. Sabrina Batonnet-Pichon, Dr. Frédérique Deshayes, Dr. Hervé Enslin and Dr. Frederic Bernard. Finally, this work would not have been possible without the pioneer works of Dr. Jean-Noël Laverrière on the regulation of gonadotrope cell genes.

AUTHOR CONTRIBUTIONS

CLC performed most of the experiments (ICF, IHF, PCR, videomicroscopy), acquired and analyzed data, interpreted data, and participated to preparation of the figures and the manuscript; EA contributed to the western blot analyses and to the preparation of the expression plasmids. VP with FP contributed to the luciferase assays and to the CRISPR-Cas9-mediated knockout experiments. SDB greatly helped with the cell motility experimental set-ups and analysis. NR and STD produced the TrkC mouse line and provided the mouse embryos. JCT contributed to data interpretation, and to preparation of the manuscript; DL was involved in all aspects of the study design, data interpretation, and manuscript preparation. All authors reviewed and commented on the paper.

FUNDING

This work was supported by grants from the Université Paris Cité, the Centre National de la Recherche Scientifique (CNRS), and the Institut National de la Santé et de la Recherche Médicale (Inserm).

COMPETING INTERESTS

The authors declare no competing interests.

ADDITIONAL INFORMATION

Supplementary information The online version contains supplementary material available at <https://doi.org/10.1038/s41420-023-01615-7>.

Correspondence and requests for materials should be addressed to David L'hôte.

Reprints and permission information is available at <http://www.nature.com/reprints>

Publisher's note Springer Nature remains neutral with regard to jurisdictional claims in published maps and institutional affiliations.



Open Access This article is licensed under a Creative Commons Attribution 4.0 International License, which permits use, sharing, adaptation, distribution and reproduction in any medium or format, as long as you give appropriate credit to the original author(s) and the source, provide a link to the Creative Commons license, and indicate if changes were made. The images or other third party material in this article are included in the article's Creative Commons license, unless indicated otherwise in a credit line to the material. If material is not included in the article's Creative Commons license and your intended use is not permitted by statutory regulation or exceeds the permitted use, you will need to obtain permission directly from the copyright holder. To view a copy of this license, visit <http://creativecommons.org/licenses/by/4.0/>.

© The Author(s) 2023